Redox Biology 20 (2019) 167–181

Contents lists available at ScienceDirect

Redox Biology

journal homepage: www.elsevier.com/locate/redox

Research Paper

Monoamine oxidase-A promotes protective autophagy in human SH-SY5Y neuroblastoma cells through Bcl-2 phosphorylation

Aslihan Ugun-Klusek[a,*], Theodosis S. Theodosi[a], Julia C. Fitzgerald[b], Florence Burté[c], Christoph Ufer[d], David J. Boocock[e], Patrick Yu-Wai-Man[f,g,h,i], Lynn Bedford[j], E. Ellen Billett[a]

[a] School of Science and Technology, Nottingham Trent University, Nottingham, UK
[b] Hertie-Institute for Clinical Brain Research, University of Tübingen and German Centre for Neurodegenerative Diseases (DZNE), Tübingen, Germany
[c] Wellcome Trust Centre for Mitochondrial Research, Institute of Genetic Medicine, Newcastle University, Newcastle Upon Tyne, UK
[d] Institute of Biochemistry, University Medicine Berlin-Charité, Berlin, Germany
[e] John van Geest Cancer Research Centre, Nottingham Trent University, Nottingham, UK
[f] NIHR Biomedical Research Centre at Moorfields Eye Hospital and UCL Institute of Ophthalmology, London, UK
[g] Cambridge Eye Unit, Addenbrooke's Hospital, Cambridge University Hospitals, Cambridge, UK
[h] MRC Mitochondrial Biology Unit, University of Cambridge, Cambridge, UK
[i] Cambridge Centre for Brain Repair, Department of Clinical Neurosciences, University of Cambridge, Cambridge, UK
[j] School of Life Sciences, University of Nottingham, Nottingham, UK

ARTICLE INFO

Keywords:
Monoamine oxidase
Autophagy
Reactive oxygen species
Neurodegeneration

ABSTRACT

Monoamine oxidases (MAOs) are located on the outer mitochondrial membrane and are drug targets for the treatment of neurological disorders. MAOs control the levels of neurotransmitters in the brain via oxidative deamination and contribute to reactive oxygen species (ROS) generation through their catalytic by-product H_2O_2. Increased ROS levels may modulate mitochondrial function and mitochondrial dysfunction is implicated in a vast array of disorders. However, the downstream effects of MAO-A mediated ROS production in a neuronal model has not been previously investigated.

In this study, using MAO-A overexpressing neuroblastoma cells, we demonstrate that higher levels of MAO-A protein/activity results in increased basal ROS levels with associated increase in protein oxidation. Increased MAO-A levels result in increased Lysine-63 linked ubiquitination of mitochondrial proteins and promotes autophagy through Bcl-2 phosphorylation. Furthermore, ROS generated locally on the mitochondrial outer membrane by MAO-A promotes phosphorylation of dynamin-1-like protein, leading to mitochondrial fragmentation and clearance without complete loss of mitochondrial membrane potential. Cellular ATP levels are maintained following MAO-A overexpression and complex IV activity/protein levels increased, revealing a close relationship between MAO-A levels and mitochondrial function. Finally, the downstream effects of increased MAO-A levels are dependent on the availability of amine substrates and in the presence of exogenous substrate, cell viability is dramatically reduced.

This study shows for the first time that MAO-A generated ROS is involved in quality control signalling, and increase in MAO-A protein levels leads to a protective cellular response in order to mediate removal of damaged macromolecules/organelles, but substrate availability may ultimately determine cell fate. The latter is particularly important in conditions such as Parkinson's disease, where a dopamine precursor is used to treat disease symptoms and highlights that the fate of MAO-A containing dopaminergic neurons may depend on both MAO-A levels and catecholamine substrate availability.

Abbreviations: 2-DG, 2-deoxy-D-glucose; Ac-DEVD-AMC, Acetyl-Asp-Glu-Val-Asp-7-amido-methyl coumarin; ATP, adenosine-5′-triphosphate; CCCP, carbonyl cyanide 3-chlorophenylhydrazone; DCDHF, 2′,7′-Dichlorodihydroflourescein diacetate; DMEM, Dulbecco's Modified Eagles Medium; DMEM/F12, Dulbecco's Modified Eagles Medium/Ham's F-12 nutrient mixture; DNPH, 2,4-Dinitrophenylhydrazine; DPBS, Dulbecco's Phosphate Buffered Saline; DTT, dithiothreitol; ETC, electron transport chain; Het, dihydroethidium; LDH, Lactate dehydrogenase; MAO, monoamine oxidase; mtDNA, Mitochondrial DNA; MTT, 3-(4,5-dimethylthiazol-2-yl)-2,5-diphenyltetrazolium bromide); NADH, ß-Nicotinamide adenine dinucleotide; PBS, phosphate buffered saline; PD, Parkinson's disease; qRT-PCR, quantitative reverse transcription PCR; RT, room temperature; ROS, reactive oxygen species; SDS-PAGE, sodium dodecyl sulphate-polyacrylamide gel; SEM, standard error of the mean

* Corresponding author.
E-mail address: aslihan.ugun-klusek@ntu.ac.uk (A. Ugun-Klusek).

https://doi.org/10.1016/j.redox.2018.10.003
Received 31 August 2018; Received in revised form 5 October 2018; Accepted 6 October 2018
Available online 09 October 2018

1. Introduction

Mitochondria play a critical role in cellular metabolism and are essential to the life of a cell. Mitochondria are the site for many important biochemical processes such as oxidative phosphorylation, β-oxidation of fatty acids, tricarboxylic acid cycle and calcium homeostasis. The process of oxidative phosphorylation relies on the coordinated transfer of electrons via the electron transport chain (ETC) components to molecular oxygen; however, during this process reactive oxygen species (ROS) are also produced as metabolic by-products [1]. Mitochondrial ROS are involved in cellular signalling but, depending on their levels, also have the potential to damage a wide variety of macromolecules including proteins, lipids and nucleic acids [2–4]. Furthermore, continuous ROS exposure can affect ETC activity and energy production, and hence mitochondrial dysfunction is implicated in a wide range of disorders including neurodegenerative diseases, cancers as well as the aging process [5].

The main source of ROS in the mitochondria is electron leak from the ETC, but ROS production also takes place outside the ETC on the mitochondrial outer membrane by monoamine oxidases (MAOs) [6]. MAOs exist as two isoforms, MAO-A and MAO-B, coded for by two separate genes and defined by their substrate and inhibitor specificities [7,8]. MAO-A is a key enzyme for the degradation of brain serotonin and norepinephrine; on the other hand, MAO-B shows greater affinity for benzylamine and phenylethylamine. Dopamine and tyramine show similar affinities for both isoforms. The oxidative deamination of monoamines produce corresponding aldehydes and hydrogen peroxide (H_2O_2) as by-products [9].

MAO inhibitors are in clinical use for the treatment of psychiatric and neurological disorders including Parkinson's disease (PD) [10]. MAOs are mainly responsible for maintaining neurotransmitter homeostasis but due to ROS production have also been implicated in cell death mechanisms and mitochondrial function [11–16]. We have previously demonstrated that MAO-A knock down in human neuroblastoma cells halves the levels of basal ROS, increases complex I activity and increases levels of ATP [11]. In addition, ETC Complex I, III and IV inhibition (known to increase ROS levels) results in increased MAO-A protein levels and MAO-A knock down protects cells against inhibitors of the ETC [11].

Mitochondria are equipped with various quality control mechanisms (antioxidant enzymes, mitochondrial proteases, fission and fusion) to prevent accumulation of damage. Furthermore, when the damage becomes too extensive, mitochondria can be degraded through selective autophagy. Acting as second messengers, ROS may play key roles in controlling cell death and survival via regulating apoptosis and autophagy [17]. Interestingly, recent research suggests a potential role for MAO-A in autophagy in prostate cancer cells and cardiomyocytes [18,19]. Increased MAO-A levels activated autophagy in prostate cancer cells, whilst in cardiomyocytes they caused the opposite effect, namely disruption of the autophagic flux. These contrary effects are not surprising since, depending on the levels, ROS can activate or interfere with quality control mechanisms and physiological ROS levels and types vary in different cells and organs [20].

In neuronal cells, ETC complex inhibition and other stressors induce transient MAO-A levels/activity [13–15] but the effects of a sustained increase in MAO-A levels and MAO-A generated ROS have not been investigated. Here, using human SH-SY5Y neuroblastoma cells overexpressing MAO-A as a cellular model, we assess the effects of sustained ROS production by MAO-A on the outer mitochondrial membrane on mitochondrial function and autophagy.

For the first time we report that, despite increased mitochondrial fragmentation in response to increased MAO-A levels, cells maintain mitochondrial membrane potential and ATP levels, possibly via ETC compensation and that mitochondrial quality control is maintained by activation of autophagy mediated through Bcl-2 phosphorylation and associated increase in Beclin 1 levels. Moreover, we show that increased MAO-A levels cause mitochondrial fragmentation in the absence of mitochondrial uncouplers.

2. Materials and methods

2.1. Reagents

^{14}C-labelled tyramine hydrochloride, oligomycin, 2-deoxy-D-glucose (2-DG), pyruvate, carbonyl cyanide 3-chlorophenylhydrazone (CCCP) and clorgyline were purchased from Sigma Aldrich (Poole, UK). Dihydroethidium (Het) and MitoTracker red were purchased from Thermo Fisher Scientific (Paisley, UK). 2′,7′-Dichlorodihydroflourescein diacetate (DCDHF) was purchased from Alexis Biochemicals (Nottingham, UK). Bafilomycin A_1 was purchased from Enzo Life Sciences (UK) Ltd. (Exeter, UK). Oligonucleotides were obtained from Biotez (Berlin, Germany).

2.2. Antibodies

LC3B (L7543) antibody was purchased from Sigma Aldrich (Poole, UK). Anti-SQSTM1/p62 (ab56416), MitoProfile® total OXPHOS human antibody cocktail (ab110411), MitoProfile® total OXPHOS rodent antibody cocktail (ab110413) and MT-ND1 (ab181848) antibodies were purchased from Abcam (Cambridge, UK). β-actin (sc-47778), Tubulin (sc-23948), Cytochrome c oxidase 1 (sc-8385), Citrate Synthase (sc-390693), MAO-A (sc-20156), Drp1 (sc-271583), Bcl-2 (sc-509) antibodies were purchased from Santa Cruz Biotechnology (Dallas, USA). Caspase 3 (GTX110543) antibody was purchased from GeneTex, Inc. (Irvine, USA). Phospho-Drp1 (Ser616, #3455), phospho-Bcl-2 (Ser70, #2827), VDAC (#4661), GAPDH (#2118), COX IV (#4844), K63-linkage specific polyubiquitin (D7A11, #5621) antibodies were purchased from Cell Signaling Technology, Inc. (Danvers, USA). OPA1 (612606) antibody was purchased from BD Biosciences (Oxford, UK), Beclin 1/ATG6 (NB500-249) antibody was purchased from Novus Biologicals (Abingdon, UK). Ubiquitin (P4D1) antibody was purchased from Enzo Life Sciences (UK) Ltd. (Exeter, UK). Anti-MAO-A (6G11-E1) monoclonal antibody was made in our laboratory. Anti-mouse IgG (#7076) and anti-rabbit IgG (#7074), HRP-linked secondary antibodies were purchased from Cell Signaling Technology Inc. (Danvers, USA). Alexa Fluor® FITC/TRITC-conjugated anti-mouse, rabbit and goat immunoglobulin G were purchased from Fisher Scientific UK Ltd. (Loughborough, UK).

2.3. Cell culture

Human SH-SY5Y neuroblastoma cells were obtained from the European Collection of Animal Cell Cultures (Salisbury, UK). SH-SY5Y cells were seeded at a density of approximately 4×10^4 cells/cm^2 on plastic culture plates or flasks (Sarstedt, Nümbrecht, Germany). Cells were grown to 75–80% confluence in Dulbecco's Modified Eagles Medium/ Ham's F-12 nutrient mixture (DMEM/F12) containing 10% foetal bovine serum, 2 mM L-glutamine, 1% non-essential amino acid solution, 100 units /ml penicillin and 100 μg/ml streptomycin at 37 °C in a 5% CO_2 humidified atmosphere.

2.4. Overexpression of MAO-A in SH-SY5Y cells

Human MAO-A was stably over expressed in the human neuroblastoma SH-SY5Y cell line by cloning human MAO-A cDNA into the expression vector (pcDNA3.1-, Invitrogen, Karlsruhe, Germany), which was then transformed into competent bacteria. The expressed plasmid DNA was purified using DNA mini and DNA midi kits (Qiagen, Manchester, UK) and SH-SY5Y cells were transfected with 1 μg of pcDNA3.1(-) containing the hMAO-A insert or 1 μg of the empty pcDNA3.1(-) vector via electroporation using the Amaxa nucleofection system (Amaxa, Cologne, Germany). Electroporated SH-SY5Y cells were

seeded in 6-well tissue culture plates in normal growth medium, which was replaced after 24 h. 48 h post-transfection, cells were passaged and seeded at 25% confluence in growth medium containing G418 sulphate (geneticin) at a concentration of 700 μg/ml. Stable SH-SY5Y clones were selected by their resistance to geneticin, which is conferred by the plasmid vector pcDNA3.1. The medium was replaced every 3–4 days until resistant foci were visible. Resistant cells were diluted in 96 well plates at a density of 0.5 cell/well and single clones were expanded and assayed for MAO-A expression.

2.5. Quantitative reverse transcription PCR (qRT-PCR)

Total RNA was isolated using the RNeasy Mini Kit (Qiagen, Manchester, UK) and was reversely transcribed into the corresponding cDNA using oligo d(T)18 and Superscript II reverse transcriptase (Invitrogen, Karlsruhe, Germany) according to the vendor's instructions. Quantitative PCR was carried out as detailed previously [11].

2.6. Gel electrophoresis and western blotting

Cells were extracted in 150 μl extraction buffer (50 mM Tris, pH 6.8, 150 mM NaCl, 5 mM EDTA, 1 mM Na orthovanadate, 0.5% Triton X-100, 2 mM PMSF and 0.2% protease inhibitor cocktail) and incubated on ice for 20 min. Samples were sonicated (3 × 3 s pulses at 60 Hz) and centrifuged for 10 min at 300 × *g* at 4 °C. Protein content was determined by using the Bio-Rad protein assay (Bio-Rad Laboratories Ltd., Hertfordshire, UK) and equal protein aliquots per sample were subjected to electrophoresis on a 10% or 12% sodium dodecyl sulphate-polyacrylamide gel (SDS-PAGE). Separated proteins were transferred onto a nitrocellulose or PVDF membrane using the Trans-Blot Turbo Transfer System (Bio-Rad Laboratories Ltd., Hertfordshire, UK). Protein loading assessed by staining with 0.05% copper phthalocyanine in 12 mM HCl. Blotted membranes were blocked for 1 h in 3% dried skimmed milk in TBS containing 0.1% Tween-20 and incubated overnight at 4 ^{0}C with primary antibodies. Membranes were washed and incubated for 2 h at room temperature (RT) with horseradish peroxidise conjugated anti-mouse or anti-rabbit immunoglobulin G. Antibody binding was revealed with Clarity ECL Substrate (Bio-Rad Laboratories Ltd., Hertfordshire, UK). Digital images were captured using Fuji Film LAS-3000 or LAS-4000 Cooled CCD Camera Gel Documentation System (Raytek Scientific Ltd., Sheffield, UK) and band intensity quantified using Aida software (Version 4.03.031, Raytest GmbH, Straubenhardt, Germany); signal intensity was normalised to total protein (quantified using copper phthalocyanine) for each well.

2.7. Immunocytochemistry

Cells were fixed on glass coverslips using 90% methanol in phosphate buffered saline (PBS) for 30 min at − 20 °C. Fixed cells were permeabilised using 0.5% Triton X-100 in PBS for 5 min at RT, then washed in PBS before blocking with 20% (v/v) normal swine serum in PBS for 30 min at RT. Slides were incubated overnight in primary antibody, washed in PBS and then incubated with secondary antibodies (Alexa Fluor® FITC/TRITC-conjugated) in 5% (v/v) normal swine serum in PBS for 30 min at RT. The slides were washed again in PBS and mounted on glass slides using Vectashield™ mounting medium (Vector Laboratories Ltd., Peterborough, UK). Confocal images were obtained using a Zeiss 510 uv–vis CLSM equipped with a META detection system and a 403 oil immersion objective. Illumination intensity was kept to a minimum (at 0.1–0.2% of laser output) to avoid phototoxicity, and the pinhole was set to give an optical slice of 2 μm.

2.8. Detection of ROS

Cells were grown to ~70–80% confluence on Lab-Tek (NUNC, Roskilde, Denmark) chamber slides and treated with clorgyline (MAO-A inhibitor) for 2 h where applicable. Media were removed and replaced with DMEM containing 100 μM DCDHF and incubated at 37 °C for 50 min. Dye was removed and replaced with Hanks buffered salt solution (HBSS) alone or HBSS plus treatment. Changes in DCDHF fluorescence (Excitation 502 nm/Emission 523 nm) were immediately monitored using a Leica CLSM inverted confocal laser scanning microscope. Images in each independent experiment were obtained using the same laser power, gain and objective.

For measurement of cellular ROS production, Het fluorescence measurements were obtained on an epifluorescence inverted microscope equipped with a 20× fluorite objective. 2 μM Het was present in the solution during the experiment, and to limit the intracellular accumulation of oxidized products no pre-incubation was used. Oxidation of Het was monitored and rates of oxidation in control and MAO-A + cells were compared. All imaging data were collected and analysed using software from Andor (Belfast, UK).

2.9. Detection of protein oxidation

Changes in oxidatively modified protein levels were observed using the Oxyblot protein oxidation detection kit (Millipore UK Limited, Hertfordshire, UK) and western blotting. Cells were extracted as described above except extraction buffer also contained 50 mM dithiothreitol (DTT) as a reducing agent to prevent the oxidation of proteins that may occur after cell lysis. Oxyblot analysis detects protein carbonyl formation, the carbonyl groups are derivatised with 2,4-Dinitrophenylhydrazine (DNPH) and then detected by antibodies (supplied with the kit) specific to the attached DNP moiety of the proteins; buffer only (without DNPH) derivatisation was used as a negative control.

2.10. Monoamine oxidase (MAO) activity assay

MAO activity was monitored using a radiometric assay with ^{14}C-labelled tyramine hydrochloride as substrate as previously described [11]. Data were normalised for protein content and rates expressed as disintegrations of ^{14}C/min/mg protein. For assessment of effects of hydrogen peroxide on MAO activity, human recombinant MAO-A (M7316, Sigma Aldrich, Dorset, UK) was re-suspended in 50 mM HEPES buffer pH 7.4. Hydrogen peroxide was added to samples to give a range of final concentrations (0.1–10 mM) while mixing on a shaker and incubated at 37 °C for 30 min. A control sample without hydrogen peroxide was also prepared in HEPES buffer.

2.11. Lactate dehydrogenase (LDH) activity

LDH activity was determined using a spectrophotometric method that quantifies the conversion of pyruvate to lactate. Samples were treated with hydrogen peroxide in the same manner as MAO-A enzyme (detailed above). Following incubation with hydrogen peroxide or buffer only (controls) LDH activity was measured. Briefly, 800 μl of 50 mM HEPES buffer, pH 7.4 (pre-warmed to 37 °C), 50 μl of 27 mM pyruvate and 50 μl of 4 mM reduced ß-Nicotinamide adenine dinucleotide (NADH) and 100 μl of sample were successively added in to a quartz cuvette. The decrease of absorbance due to the oxidation of NADH was recorded every 5 s for 5 min in a Beckman Coulter DU 530 Life Science UV/VIS Spectrophotometer at 340 nm. LDH activity was calculated from the slope of the absorbance curve.

2.12. Caspase-3 activity assay

Caspase-3 activity was monitored using Acetyl-Asp-Glu-Val-Asp-7-amido-methyl coumarin (Ac-DEVD-AMC, Sigma Aldrich, Dorset, UK) as a substrate. Cells were harvested by centrifugation at 300 × *g* for 5 min. The pellet was washed twice with DMEM, resuspended in 200–300 μl lysis buffer (50 mM HEPES, 5 mM CHAPS, 5 mM DTT, pH 7.4) and

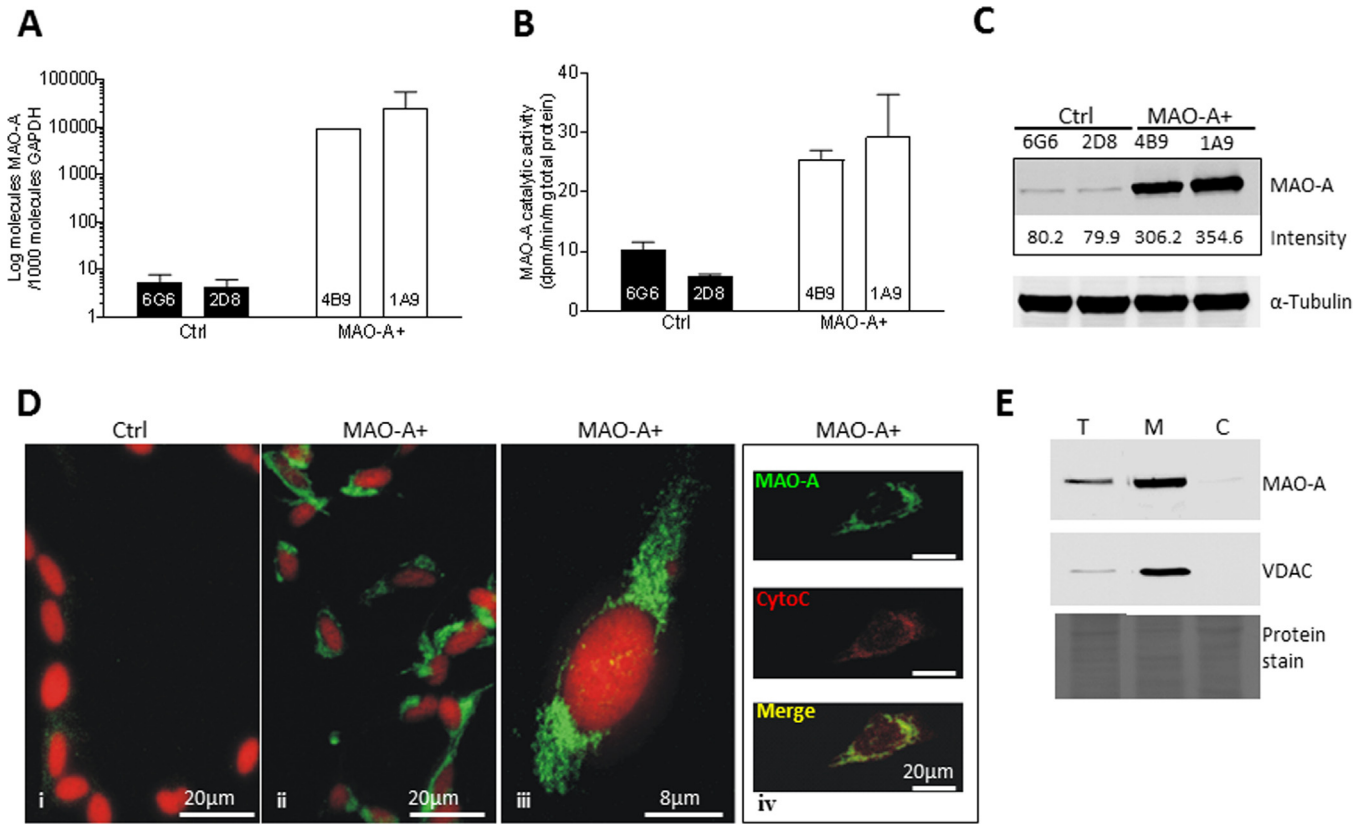

Fig. 1. Characterisation of SH-SY5Y clones overexpressing MAO-A (A) MAO-A mRNA expression was measured by qRT-PCR in stable SH-SY5Y cell control (Ctrl) and MAO-A overexpressing (MAO-A+) clones. (B) MAO catalytic activities were measured in Ctrl and MAO-A+ cells via a radiometric method using ^{14}C-Tyramine as a substrate and are expressed as disintegrations (dpm) of ^{14}C/min/mg total protein ± SEM. MAO-A activity is increased 2.5–5.1 fold in MAO-A+ clones. (C) Western blot analyses of MAO-A protein levels in Ctrl and MAO-A+ clones confirming increased MAO-A protein levels in MAO-A+ clones. MAO-A protein levels increased 3.8–4.4 fold in the MAO-A+ clones, band intensities are indicated under each lane. Tubulin used to confirm equal loading. (D) Representative confocal images showing MAO-A protein (green) using immunocytochemistry in Ctrl (panel i) and MAO-A+ cells (panel ii). Nuclei are counterstained with propidium iodide (red). Photomicrographs are representative of > 6 independent experiments. Panel iii shows an enlarged view of an MAO-A overexpressing cell. Panel iv shows mitochondrial localisation of MAO-A protein in MOA-A+ cells by double immunofluorescent labelling of MAO-A (green) and cytochrome c oxidase (red). Panels show ×63 magnification with zoom. (E) Western blot analyses of MAO-A protein in MAO-A+ cells in total cell homogenate (T), mitochondria enriched (M) and cytosolic (C) fractions demonstrating MAO-A protein continues to localise to the mitochondria; mitochondrial outer membrane protein VDAC is used to demonstrate fractionation efficiency, equal protein loading is demonstrated by total protein staining by copper phthalocyanine. Error bars represent SEM of n = 3.

incubated on ice for 20 min. The lysates were centrifuged at 200 × *g* at 4 °C for 5 min to remove cell debris. Cell lysates were transferred to black 96-well plates and made up to 80 µl with assay buffer (20 mM HEPES pH 7.4, 0.1% CHAPS, 5 mM DTT, 2 mM EDTA). Reactions were initiated by the addition of AC-DEVD-AMC to a final concentration of 200 µM in a total reaction volume of 100 µl. Fluorescence was read in the BMG CLARIOstar UV/vis spectrometer (BMG Labtech, UK) with excitation at 360 nm and emission at 460 nm every 5 min for 4 h at 37 °C. Data were normalised for protein content and expressed as Δ fluorescence units/min/µg protein.

2.13. Mitochondrial network analysis

1×10^5 cells were seeded on glass bottom dishes and incubated in MitoTracker red (75 nM) at 37 °C for 30 min. Cells were washed with PBS and imaged in MEM without phenol red (Thermo Fisher Scientific, Paisley, UK) supplemented with 25 mM HEPES. Live cells were imaged at RT using an A1R point-scanning inverted confocal microscope (Nikon, UK) taking a total of 69 z-stacks with step intervals of 0.11 µm using a high speed piezo Z stage. Individual images were deconvolved and analysed using the DeConvolution and Object Analyzer algorithms from the Huygens Essential software (Scientific Volume Imaging, The Netherlands). The mean number, volume and length of objects per cell were measured and compared using Mann-Whitney-Wilcoxon *U*-test.

2.14. Mitochondrial DNA (mtDNA) quantification

Total DNA was extracted from cell pellets using the DNeasy Blood and tissue purification kit (Qiagen, Manchester, UK). Quantification of mtDNA was carried out as previously described [21] using a probe-based multiplex Taqman real-time PCR assay [22]. Briefly, triplex reactions amplified MTND1, MTND4 and B2M using iTaq Supermix following the manufacturer's instructions (Bio-Rad Laboratories Ltd., Hertfordshire, UK). The mean mtDNA copy number and mtDNA deletion levels were calculated using the 2-ΔCt method obtained from MTND1-B2M and MTND1-MTND4 ΔCt value, respectively.

2.15. Mitochondria preparation

Mitochondrial fractions from human SH-SY5Y neuroblastoma cells were prepared as previously described [23].

2.16. ETC complex activities

The activities of the mitochondrial ETC complexes and the matrix marker enzyme, citrate synthase, were determined following the protocols described for cultured cells by Spinazzi et al., with minor modifications [24]. Mitochondrial fractions were prepared and stored at − 80 °C. Initial experiments were carried out to optimise sample

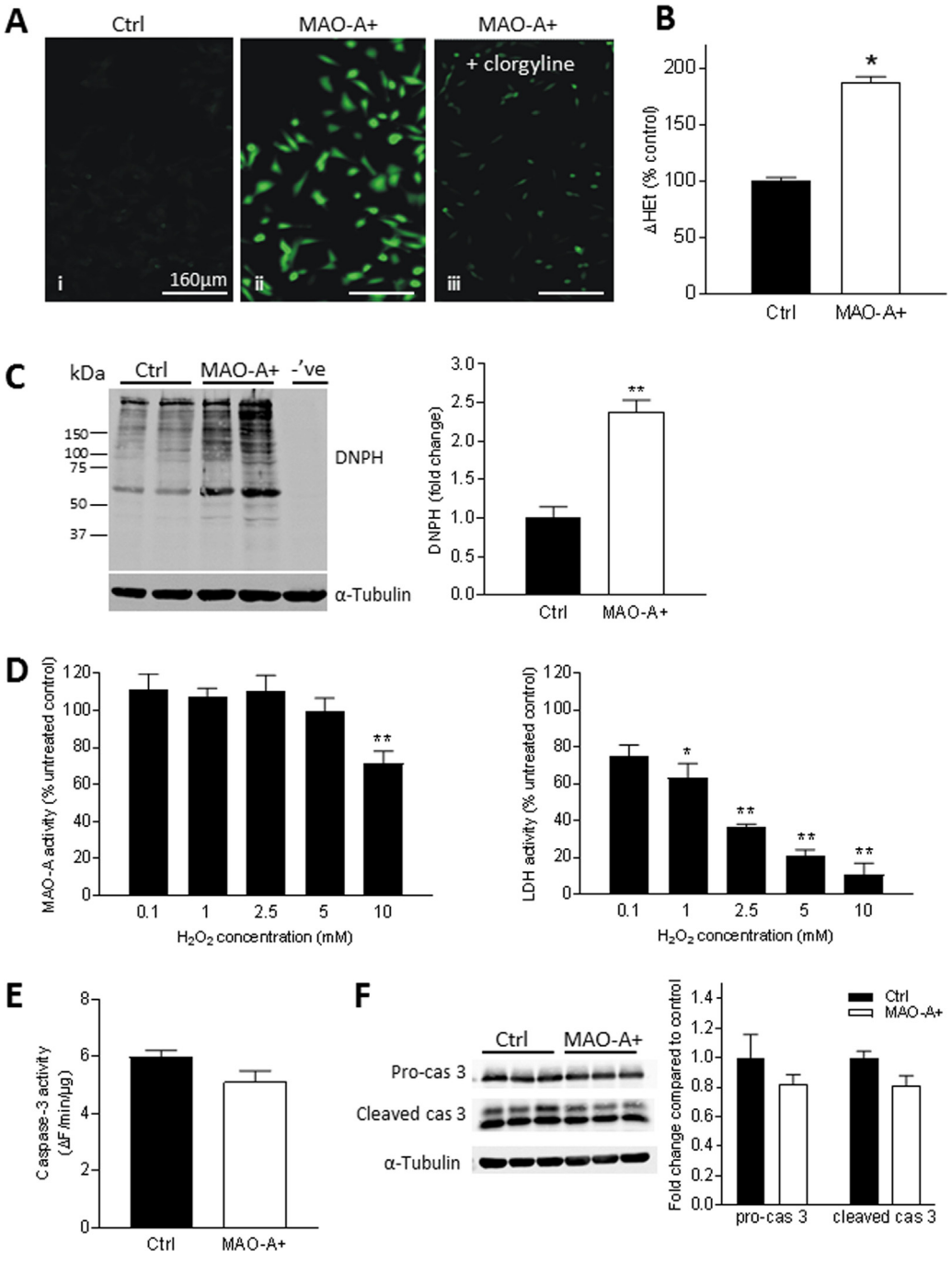

Fig. 2. MAO-A overexpression results in increased basal reactive oxygen species (ROS) levels. (A) DCDHF fluorescent probe was employed to monitor ROS levels in live cultures of Ctrl (panel i) and MAO-A + (panels ii and iii) cells. Cells were incubated with 100 µM DCDHF at 37 °C for 50 min, dye was then removed and changes in DCDHF fluorescence (Excitation 502 nm/Emission 523 nm) were immediately monitored using a Leica CLSM inverted confocal laser scanning microscope. For inhibiting MAO-A activity, cells were pre-treated with 1 µM clorgyline (MAO-A inhibitor) for 2 h (panel iii). Representative images are shown; images in each independent experiment were taken using the same laser power, gain and objective. **(B)** For Het fluorescence measurements 2 µM Het was present in the solution during the experiment but no pre-incubation was used. Epifluorescence inverted microscope equipped with a 20× fluorite objective was used to obtain measurements. Oxidation of Het was monitored and rates of oxidation in control and MAO-A + cells were compared. **(C)** Oxyblot protein oxidation detection kit and Western blotting analyses were used to observe oxidatively modified protein levels in Ctrl and MAO-A + cells. The carbonyl groups are derivatized with 2,4-Dinitrophenylhydrazine (DNPH) and then detected by antibodies (supplied with the kit) specific to the attached DNP moiety of the proteins. Increased protein carbonylation detected in MAO-A + cells ($p = 0.0032$). Buffer only derivatization of MAO-A + cell extract serves as a negative control (-'ve). **(D)** Recombinant MAO-A and LDH activity was measured in the presence of H_2O_2. Enzyme was re-suspended in assay buffer and incubated with a range of H_2O_2 (0.1–10 mM) or in assay buffer (as control) at 37 °C for 30 min prior to activity assay. Results are shown as mean % untreated control ± SEM for three independent experiments ($n = 3$). One-way ANOVA with Dunnett's multiple comparison test were performed to assess the effects of H_2O_2 on MAO-A and LDH enzyme activity. **(E)** Apoptotic cell death in Ctrl and MAO-A + cells was assessed by caspase-3 activity using Acetyl-Asp-Glu-Val-Asp-7-amido-methyl coumarin (Ac-DEVD-AMC) as a substrate. Fluorescence was read with excitation at 360 nm and emission at 460 nm every 5 min for 4 h at 37 °C. Data were normalised for protein content and expressed as Δ fluorescence units/min/µg protein, where $n = 5$. **(F)** Western blot analyses of pro- and cleaved caspase 3 protein levels in Ctrl and MAO-A + cells. Band intensities are quantified and normalised to total protein levels and are shown as a fold change compared to Ctrl cells. For cleaved caspase 3 total of doublet band intensity (detected at 17/19 kDa) was used. Student's T-tests were performed to compare caspase 3 levels. Tubulin is used to confirm equal loading. Error bars represent SEM of $n = 3$. *$P < 0.05$, **$P < 0.01$.

protein content in the absence and presence of inhibitors to each complex. Assay volumes were adjusted to 200 µl final volume and contained 30 µg (for complex I assay) or 4 µg (for citrate synthase, complex II, III and IV assays) of mitochondrial fractions. Enzyme activity assays were performed using 96 well microplates simultaneously for control and MAO-A overexpressing cells using BMG CLARIOstar UV/vis spectrometer (BMG Labtech, UK).

2.17. Proteomics analysis of ETC subunits

Cells were cultured as described above and cell pellets were extracted in 9.5 M urea, 2% DTT and 1% N-Octyl-Beta-Glucopyranoside by 3 rounds of freeze-thaw cycles. Cell extracts were sonicated (3 × 5 s pulses at 60 Hz) and centrifuged at 10,000 × *g* at 4 °C for 5 min. 50 µg of the supernatants were adjusted to 20 µl and processed for trypsin digestion and SWATH-MS analysis as described previously [25]. A spectral library for SWATH extraction was constructed using the output from ProteinPilot 5.01 (SCIEX, Framingham, USA) combining 5

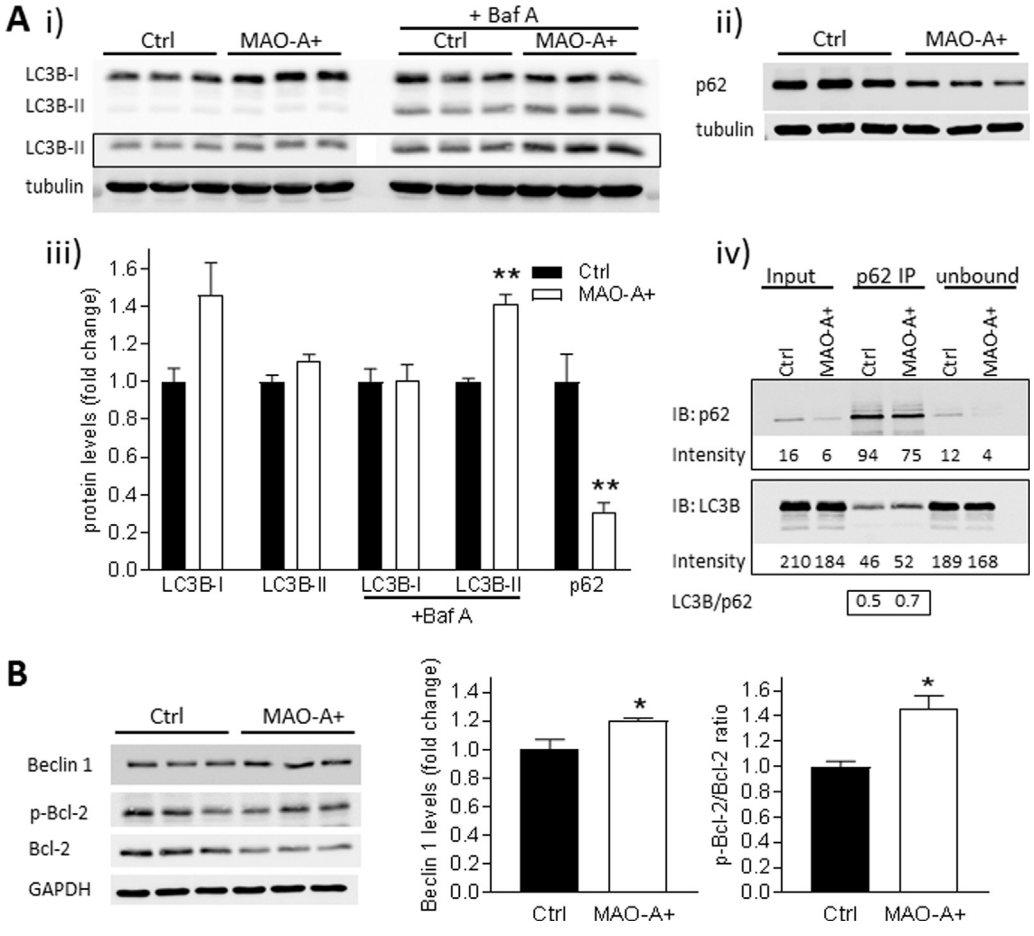

Fig. 3. MAO-A overexpression activates autophagy through phosphorylation of Bcl-2. (A) LC3B-I and LC3B-II protein levels in Ctrl and MAO-A+ cells in presence and absence of Bafilomycin A_1 (BafA, 100 nM) treatment monitored using Western blotting. Long exposure for LC3B-II is shown in the box (i). Basal P62 protein levels in Ctrl and MAO-A+ cells monitored using Western blotting (ii). Band intensities are quantified and normalised to total protein levels and are shown as a fold change compared with Ctrl cells (iii). Tubulin used to confirm equal loading. MAO-A+ cells had significantly more LC3B-II following Bafilomycin A_1treatment ($p = 0.002$) and lower basal p62 levels ($p = 0.01$). Immunoprecipitation of Ctrl and MAO-A+ cell homogenates with p62 antibody followed by Western blotting with p62 and LC3B antibodies (iv). Band intensities are indicated under each lane. More LC3B immunoprecipitated with p62 in MAO-A+ cells (LC3B/p62 ratio is increased from 0.5 in control cells to 0.7 in the MAO-A+ cells) showing increased p62-LC3B interaction. **(B)** Representative immunoblots and quantification of Beclin 1, phosphorylated Bcl-2 (p-Bcl-2) and Bcl-2 levels in Ctrl and MAO-A+ cells. Beclin 1 band intensities are quantified and normalised to total protein levels and are shown as a fold change compared to Ctrl cells. Phosphorylated Bcl-2 and Bcl-2 band intensities are quantified and expressed as p-Bcl-2/Bcl-2 ratios in Ctrl and MAO-A+ cells. GAPDH was used to confirm equal loading. Error bars represent SEM of n = 3. Student's *t*-test was performed to compare Ctrl and MAO-A+. *P < 0.05.

information dependent acquisition runs per experimental group, filtered for shared peptides, and aligned to the SWATH data file using spiked in iRT peptides (Biognosys, Switzerland) using PeakView 2.1 SWATH microapp (SCIEX, Framingham, USA). SWATH data extraction, quantitation and fold change analysis were carried out using the SCIEX OneOmics cloud processing software with parameters; 6 peptides per protein, 6 transitions per peptide, 75 ppm extracted ion chromatogram and 5 min extraction width [26]. 70% confidence limit and minimum of 2 peptides per protein were used as criteria for assessing fold change.

2.18. Mitochondrial potential measurements

Mitochondrial membrane potential was assessed with the Molecular Probes™ JC-1 Dye (Fisher Scientific UK Ltd, Loughborough, UK). 1×10^5 cells were seeded on 96 well clear bottom black microplates (Corning®, Scientific Laboratory Supplies Limited, Nottingham, UK). The following day growth media was removed and cells were incubated in growth media containing JC-1 dye (4 μg/ml) at 37 °C in a 5% CO_2 humidified atmosphere for 15 min. For the positive controls 50 μM CCCP, a mitochondrial membrane disrupter was added simultaneously with JC-1. To ensure a rapid reduction in mitochondrial membrane potential a relatively high concentration of CCCP was used. Following incubation, wells were washed once and 100 μl of Hanks' Balanced Salt solution were added to each well and fluorescence was measured at excitation/emission wavelength of 490 nm/520 nm and 490 nm/590 nm. Growth media only treatment was used for background reading.

2.19. ATP measurement

ATP levels were measured using the luminescence based ViaLight® Plus assay kit (Lonza Inc., Rockland, USA). Cells were cultured in 24 well plates and once confluent, cell monolayer was washed with Dulbecco's Phosphate Buffered Saline (DPBS) and were incubated for 1 h in DMEM containing either 10 mM glucose, 10 mM glucose plus 3 μg/ml oligomycin (glycolytic ATP generation), 10 mM 2-DG plus 1 mM (or 10 mM) pyruvate (oxidative ATP production) or 10 mM 2-DG plus 1 mM (or 10 mM) pyruvate plus 3 μg/ml oligomycin. Following treatment cell monolayer was washed with DPBS, extracted in lysis buffer (provided with the kit) and assayed for ATP levels according to the manufacturer's instructions using a microplate reader (CLARIOstar, BMG Labtech, UK). ATP standards were prepared in the range of 0.5–5000 pmol/assay and results were expressed as mean ATP pmol/μg total protein. Each sample and standard was prepared in triplicate in the assay, which was performed for each independent experiment.

2.20. Immunoprecipitation

For immunoprecipitation the Invitrogen Dynabeads® co-ip kit (14321D, Thermo Fisher Scientific, Paisley, UK) was used following the manufacturer's instructions. Briefly, 5 μg of antibody was added to 1 mg of Dynabeads in coupling buffer and incubated at 37 °C overnight with rotation. Cell pellets were homogenised in extraction buffer (supplied with the kit) using a Dounce, All-Glass Tissue Grinder (Apollo Scientific, UK). Dynabeads/antibody complex was equilibrated in extraction buffer and then incubated with 3.5 mg of protein homogenate for 1 h at 4 °C with rotation. Beads were washed, co-immunoprecipitated proteins

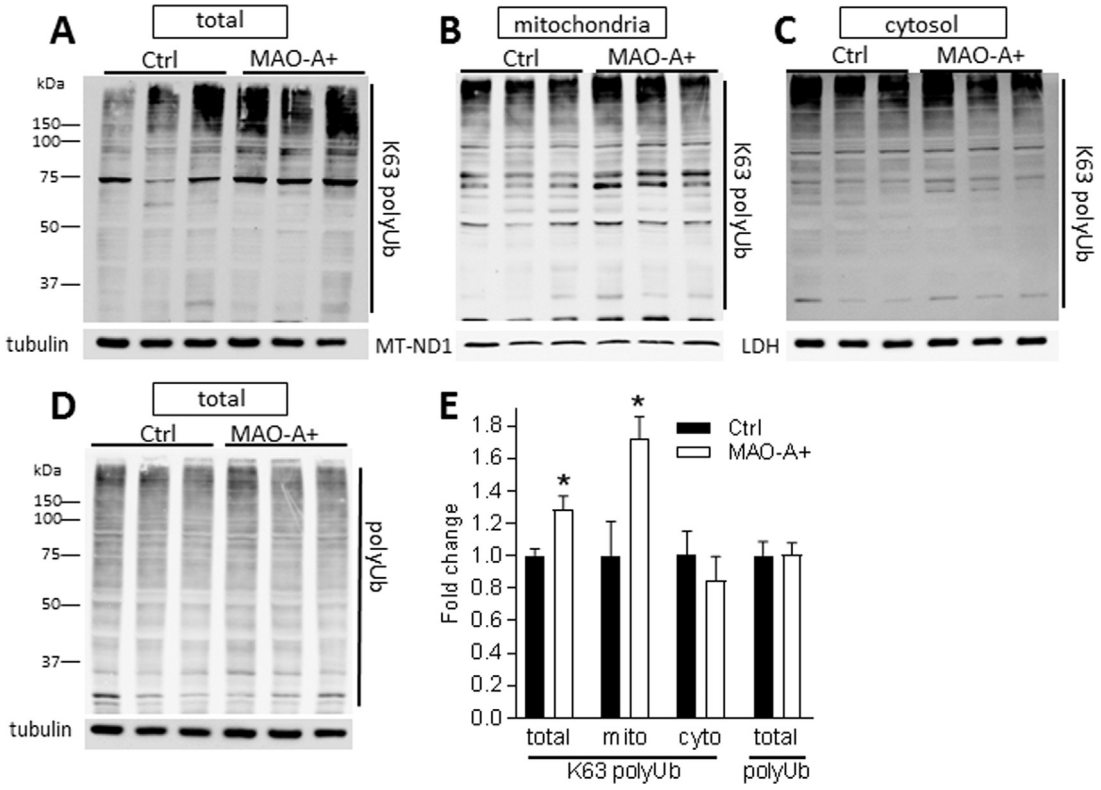

Fig. 4. MAO-A overexpression causes increased K63 ubiquitination. (A–D) K63 polyubiquitin (K63 polyUb) and polyubiquitin (polyUb) Western blots of total homogenates and K63 polyUb Western blots of mitochondrial and cytosolic fractions from Ctrl and MAO-A+ cells. K63-linkage specific polyubiquitin antibodies were used to detect K63 ubiquitination of proteins in samples. An anti-Ubiquitin antibody was used to detect all polyubiqutin chains. Tubulin, MT-ND1 and LDH used to confirm equal loading for total, mitochondrial and cytosolic fractions respectively. **(E)** Band intensities are quantified and normalised to total protein levels and are shown as a fold change compared with Ctrl cells. MAO-A+ cells have significantly higher K63 polyUb ($p = 0.037$) in total homogenates and mitochondrial fractions ($p = 0.045$). Student's *T*-tests were performed to compare Ctrl and MAO-A+. Error bars represent SEM of $n = 3$. *$P < 0.05$, **$P < 0.01$.

were eluted in the elution buffer (supplied with the kit) and analysed by Western blotting.

2.21. MTT cell viability assays

MTT (3-(4,5-dimethylthiazol-2-yl)-2,5-diphenyltetrazolium bromide) assay was used to assess the cytotoxic effects of tyramine. Cells were seeded in 96-well plates and left to recover for 24 h. Cells were treated with tyramine (0.1–1 mM) and at the end of the indicated time points cells were incubated for 1 h with MTT, the supernatant was carefully removed, and 100 µl of dimethyl sulfoxide was added to each well to dissolve the formazan product. Absorbance was recoded at 570 nm. Results were expressed as a percentage of untreated control for both control and MAO-A+ cells.

2.22. Statistical analysis

All measurements were performed in triplicate, repeated a minimum of three times and data are expressed as mean ± standard error of the mean (SEM). Statistical significance for multiple comparisons was performed using 2 way ANOVA followed by Bonferroni's multiple comparisons test. The Student's *T*-test was used to perform comparisons on other data. In all cases, $p < 0.05$ was considered significant and p values of < 0.05 and < 0.01 are marked by * and ** respectively.

3. Results

3.1. Characterisation of SH-SY5Y cells overexpressing MAO-A

SH-SY5Y cells were stably transfected with either the pcDNA3.1(-) vector lacking the MAO-A sequence, referred to as control (Ctrl) clones or with pcDNA3.1(-) containing the MAO-A cDNA sequence, referred to as MAO-A+. RNA was extracted for characterisation of MAO-A mRNA expression levels. Fig. 1A shows that MAO-A+ clones exhibited increased MAO-A mRNA expression (1900–5100 fold) compared to control SH-SY5Y clones. Individual SH-SY5Y cell clones were then expanded further and extracts taken for evaluation of MAO-A catalytic activity. MAO-A+ clones had increased MAO-A catalytic activity of at least 2.5 fold compared to the control clones (Fig. 1B). Western blot analysis confirmed the increased expression of MAO-A protein in the MAO-A+ clones (Fig. 1C). Control clone 2D8 and MAO-A+ clone 1A9 were used for further work. Immunocytochemistry verified the increased expression of MAO-A protein in the MAO-A+ cells (Fig. 1D panels i–iii) and Fig. 1D (panel iv) shows co-localisation of MAO-A protein in MAO-A+ cells with the mitochondrial enzyme cytochrome c oxidase, further signifying that overexpressed MAO-A in SH-SY5Y cells continues to localise to the mitochondria. This is also confirmed by monitoring MAO-A in mitochondrial and cytosolic fractions using Western blotting and outer mitochondrial membrane protein Voltage-dependent anion-selective channel (VDAC) protein as a control (Fig. 1E).

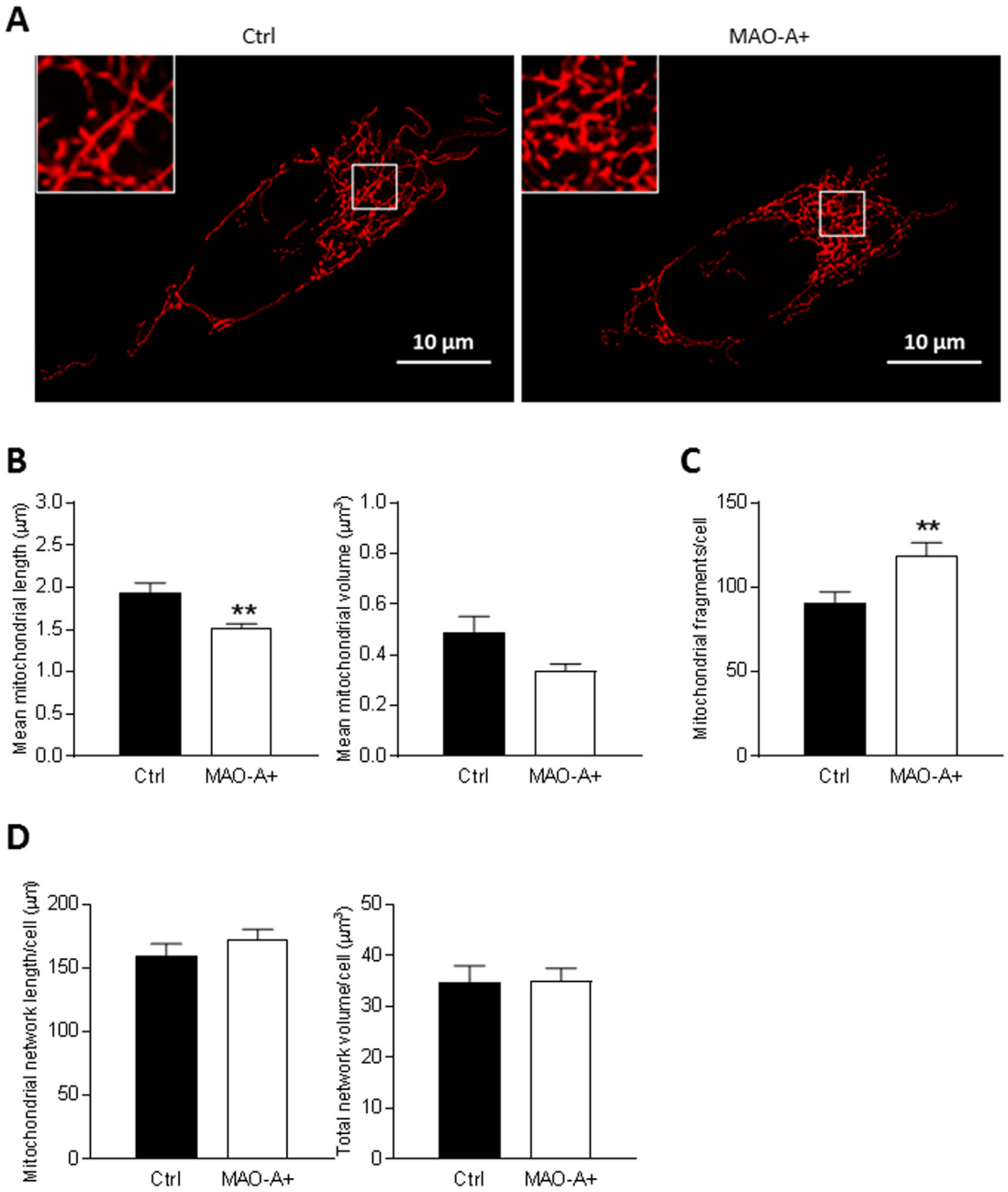

Fig. 5. MAO-A overexpression results in mitochondrial fragmentation. (A) Mitochondrial network images obtained by Mitotracker red staining. Live cells were imaged using an A1R point-scanning inverted confocal microscope. Representative images are shown. **(B–D)** 45–50 Ctrl and MAO-A+ cells were imaged and length, volume and number of objects per cell were measured using Huygens Essential software algorithms. Mann-Whitney-Wilcoxon *U*-tests were performed to compare Ctrl and MAO-A+. MAO-A+ cells had significantly reduced mitochondrial length ($p = 0.008$) and increased number of mitochondrial fragments ($p = 0.003$) but MAO-A overexpression had no effect on total mitochondrial network length ($p = 0.214$) and volume ($p = 0.477$) per cell. Error bars represent SEM. $n = 6$. *$P < 0.05$, **$P < 0.01$.

3.2. MAO-A overexpression results in increased basal reactive oxygen species (ROS) levels

The fluorescent probe DCDHF was initially employed to monitor ROS levels in live cultures of control and MAO-A+ cells (Fig. 2A). Basal levels of ROS in MAO-A+ cells were higher than in controls (Fig. 2A panels i–ii) and were reduced by clorgyline, an irreversible MAO-A inhibitor (Fig. 2A, panel iii), confirming the increased ROS in MAO-A+ cells were due to increased MAO-A activity. This finding was confirmed using the fluorescent probe Het which allows the measurement of ROS using real-time fluorescence microscopy. The rate of oxidation was found to be higher in MAO-A+ cells (Fig. 2B). Finally, Fig. 2C demonstrates that increased ROS levels in MAO-A+ cells result in increased protein carbonylation, suggesting increased protein oxidation. Next, we investigated the potential effects of this increased ROS on MAO-A enzyme catalytic activity. For this we used recombinant human MAO-A (EC 1.4.3.4) and, as a control, L-Lactic dehydrogenase (LDH, EC 1.1.1.27); each enzyme was treated with increasing concentrations (0.1–10 mM) of hydrogen peroxide (H_2O_2). LDH activity was reduced in a dose dependent manner by H_2O_2, significantly at 1 mM and higher concentrations (Fig. 2D). In comparison, MAO-A activity was only affected at 10 mM H_2O_2, indicating that MAO-A is highly resistant to this oxidant (Fig. 2D).

In this study we aimed to investigate the effects of stable

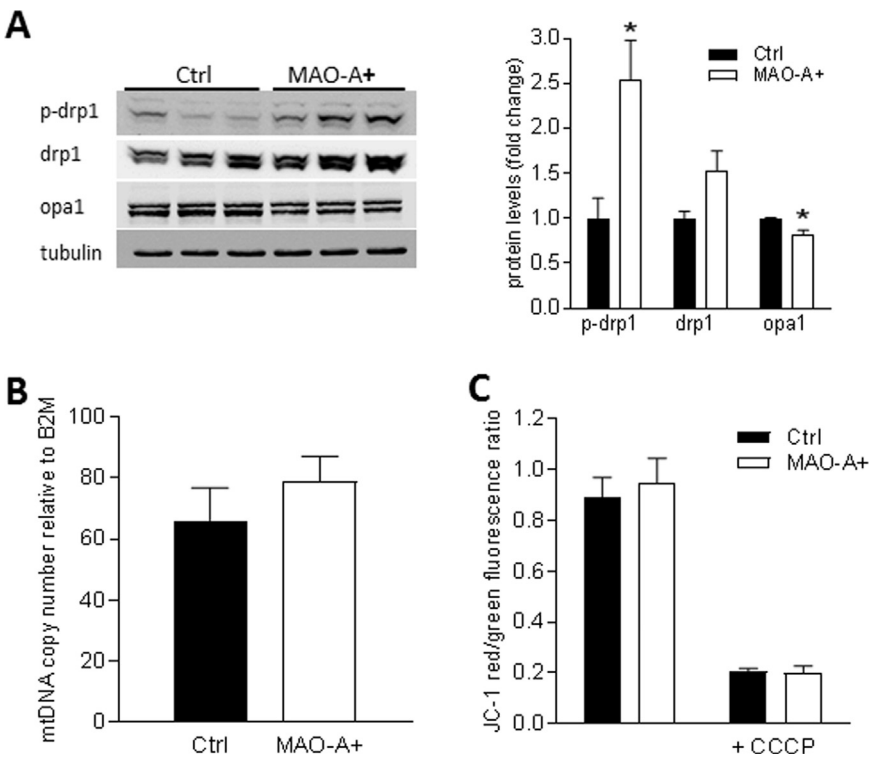

Fig. 6. MAO-A overexpression cause increased mitochondrial fission proteins. (A) Representative Western blots and quantification of phosphorylated drp1 (p-drp1), drp1 and opa1 levels in Ctrl and MAO-A+ cells. Band intensities are quantified and normalised to total protein levels and are shown as a fold change compared to Ctrl cells. Tubulin is used to confirm equal loading. **(B)** mtDNA copy number in Ctrl and MAO-A+ cells. The analysis was performed using a probe-based multiplex Taqman real-time PCR assay. MtDNA copy number was calculated using the 2-ΔCt method obtained from MTND1-B2M value for each cell line. **(C)** Mitochondrial membrane potential was assessed using JC-1 dye. Fluorescence was measured at excitation/emission wavelength of 490 nm/520 nm and 490 nm/590 nm, and red/green fluorescence ratio was compared in Ctrl and MAO-A+ cells. A mitochondrial membrane disrupter CCCP (50 μM) was used as a positive control. Error bars represent SEM of n = 3 independent experiments. Student's *t*-test was performed to compare Ctrl and MAO-A+. *P < 0.05.

overexpression of MAO-A, with associated increases in ROS levels, on cellular responses. First, we compared basal caspase 3 activity and protein levels in control and MAO-A+ cells and found that they were similar (Fig. 2E and F). This suggests that sustained ROS exposure may have induced an adaptive response, which allowed the cells to tolerate higher basal ROS levels.

3.3. Increased MAO-A expression activates autophagy

Next, we explored how MAO-A+ cells maintain cellular viability under increased oxidative stress. Since autophagy functions as a stress response and can be regulated by several intracellular stressors including oxidative stress, we investigated the effects of MAO-A overexpression on autophagy [27,28]. During autophagy, LC3-I is converted to LC3-II by lipidation and this causes LC3-II to migrate differently on SDS-PAGE. LC3-II is required for the formation of the autophagosome and accumulation of LC3-II following induction of autophagy, or interruption of autophagosome-lysosome fusion, is often used as a quantitative marker of autophagy [29]. Bafilomycin A_1 is a specific inhibitor of the vacuolar type H+-ATPase (V-ATPase) and inhibits the acidification of lysosomes, thus preventing the maturation of autophagic vacuoles [30,31]. LC3B-II levels were increased in the MAO-A+ cells compared to controls following bafilomycin A_1 treatment (Fig. 3Ai and iii), suggesting increased autophagy. Steady state levels of autophagy substrate p62 (Sequestosome-1) are suggested to reflect the autophagic state of the cells, with decreased p62 levels being associated with autophagy activation [32]. Basal levels of p62 were reduced in the MAO-A+ cells (Fig. 3Aii and iii) further supporting autophagy activation. Finally, co-immunoprecipitation experiments using antibodies against p62 indicate that, despite reduced p62 levels, increased interaction of LC3B with p62 in MAO-A+ cells (Fig. 3A iv). Overall, these results support activation of autophagy in MAO-A+ cells.

3.4. MAO-A overexpression activates autophagy through phosphorylation of Bcl-2

Previous studies suggest that dissociation of Bcl-2 from Beclin 1 is one important mechanism for activating autophagy. Beclin 1 interacts with several cofactors to regulate the lipid kinase Vacuolar protein sorting 34 (Vps34), a critical regulator of autophagy, and therefore has a central role in autophagy induction. Binding to Bcl-2 inhibits Beclin 1 but phosphorylation of Bcl-2 disrupts Bcl-2/Beclin 1 interaction leading to autophagy stimulation [33,34]. In order to study the potential mechanism of autophagy activation in MAO-A+ cells we investigated levels of Beclin 1 and phosphorylation of Bcl-2. We found a small but significant increase in Beclin 1 levels and increased phosphorylation of Bcl-2 in MAO-A+ cells (measured by p-Bcl-2/Bcl-2 ratio). Overall, these results suggest autophagy activation in MAO-A+ cells is through disrupted Bcl-2/Beclin 1 interaction (Fig. 3B).

3.5. Mitochondria are targeted for clearance via autophagy

Since Lysine 63 (K63)-linked ubiquitination of substrates is a common marker of autophagy and is suggested to be involved in clearance of damaged mitochondria, we investigated total and K63-linked ubiquitinated protein levels [35]. The levels of K63-linked ubiquitinated proteins in MAO-A+ cells were increased (Fig. 4A and E); this increase was confined to the mitochondrial fraction (Fig. 4B, C and E), suggesting that mitochondria are being targeted for autophagic clearance. There were no significant differences in the basal levels of total ubiquitinated protein pools in control and MAO-A+ cells (Fig. 4D and E).

3.6. MAO-A overexpression results in mitochondrial fragmentation

Next we investigated how sustained overexpression of MAO-A influences the structure of the mitochondrial network and its function. Fig. 5A demonstrates representative images showing mitochondrial networks in control and MAO-A+ cells. MAO-A overexpression resulted in a reduced mean mitochondrial length and volume (Fig. 5B) but had no effect on total mitochondrial network length and volume per cell (Fig. 5D). Accordingly, the number of mitochondrial fragments in MAO-A+ cells was increased (Fig. 5C).

To further characterise mitochondrial network changes we

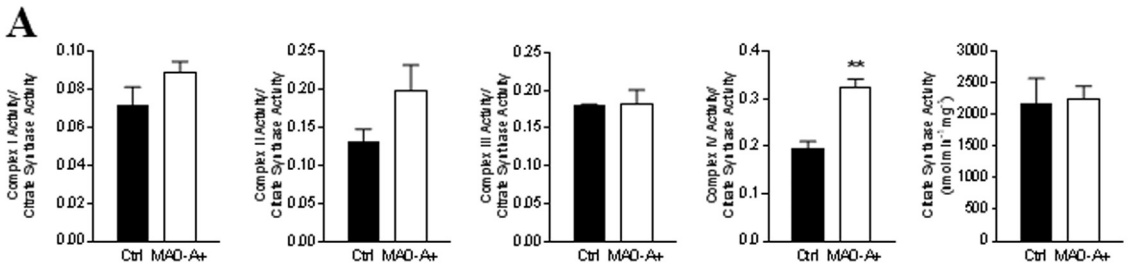

B

Gene name	Protein name	Accession no	Fold change	Number of peptides detected
COX4I1	Cytochrome c oxidase subunit 4I1	P13073	1.43	6
COX5A	Cytochrome c oxidase subunit 5A	P20674	NS	10
COX5B	Cytochrome c oxidase subunit 5B	P10606	2.06	7
COX6B1	Cytochrome c oxidase subunit 6B1	P14854	1.99	4
COX6C	Cytochrome c oxidase subunit 6C	P09669	2.20	7
COX7A2	Cytochrome c oxidase subunit 7A2	P14406	2.08	3
MT-CO2	Mitochondrially encoded cytochrome c oxidase II	P00403	2.58	6

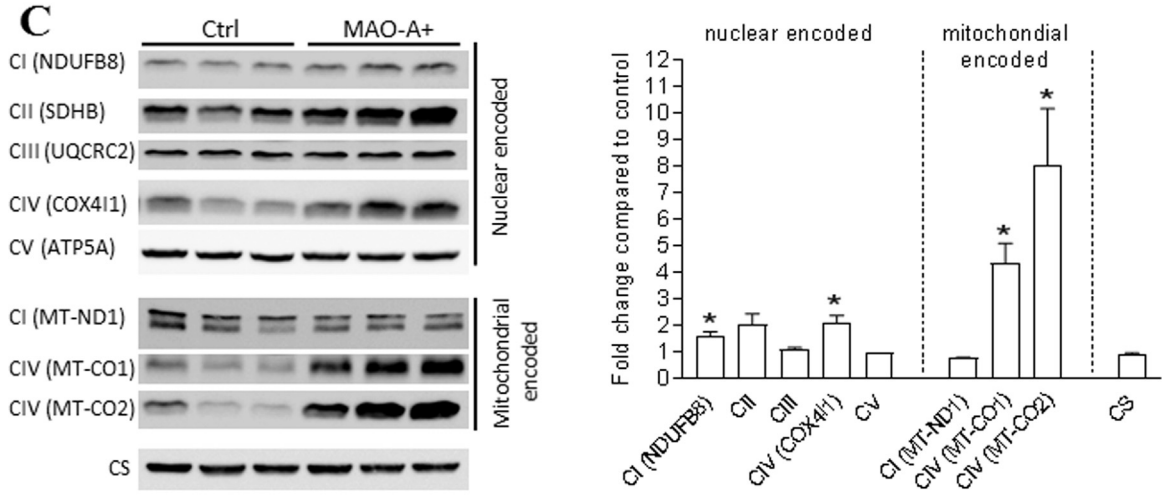

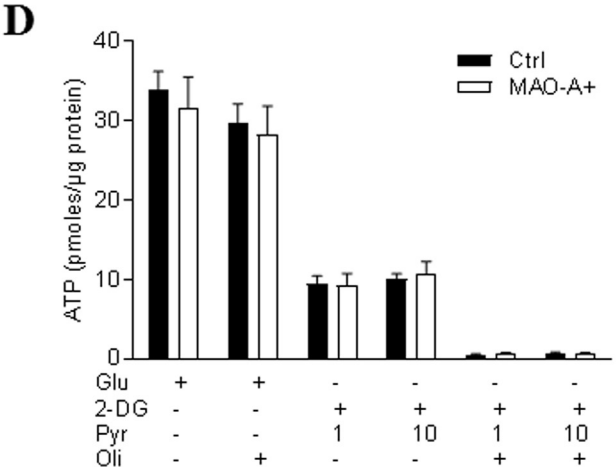

Fig. 7. Effects of MAO-A overexpression on mitochondrial electron transport chain and ATP. (A) Complex I–IV and citrate synthase activities were assessed in mitochondria enriched fractions of Ctrl and MAO-A+ cells. MAO-A+ cells had significantly higher Complex IV activity ($p = 0.004$). **(B)** Differentially expressed mitochondrial respiratory chain complex IV subunits detected using SWATH mass spectrometry analysis. Seven complex IV subunits were detected, six of the complex IV subunits showed a 1.43–2.58 fold increase in MAO-A+ cells. **(C)** Complex I–V and citrate synthase (CS) protein levels in Ctrl and MAO-A+ cells monitored using Western blotting. Blots were probed with an antibody cocktail directed to subunits of complex I (NDUFB8), complex II (SDHB), complex III (UQCRC2), complex IV (cytochrome c oxidase subunit II, MT-CO2), and complex V (ATP5A). Same samples were also probed with antibodies directed to CI (MT-ND1), CIV (cytochrome c oxidase subunit I, MT-CO1) and Citrate synthase (CS). Band intensities are quantified. Student's *t*-test was performed to compare Ctrl and MAO-A. **(D)** ATP levels were measured using a luminescence based assay. Cells were incubated for 1 h in DMEM containing either 10 mM glucose (Glu), 10 mM glucose plus 3 µg/ml oligomycin (oli) (glycolytic ATP generation), 10 mM 2-deoxyglucose (2-DG) plus 1 mM (or 10 mM) pyruvate (Pyr) (oxidative ATP production) or 10 mM 2-DG plus 1 mM (or 10 mM) pyruvate plus 3 µg/ml oligomycin. Student's *t*-test was performed to compare Ctrl and MAO-A+. Error bars represent SEM of n = 3 independent experiments. *$P < 0.05$, **$P < 0.01$.

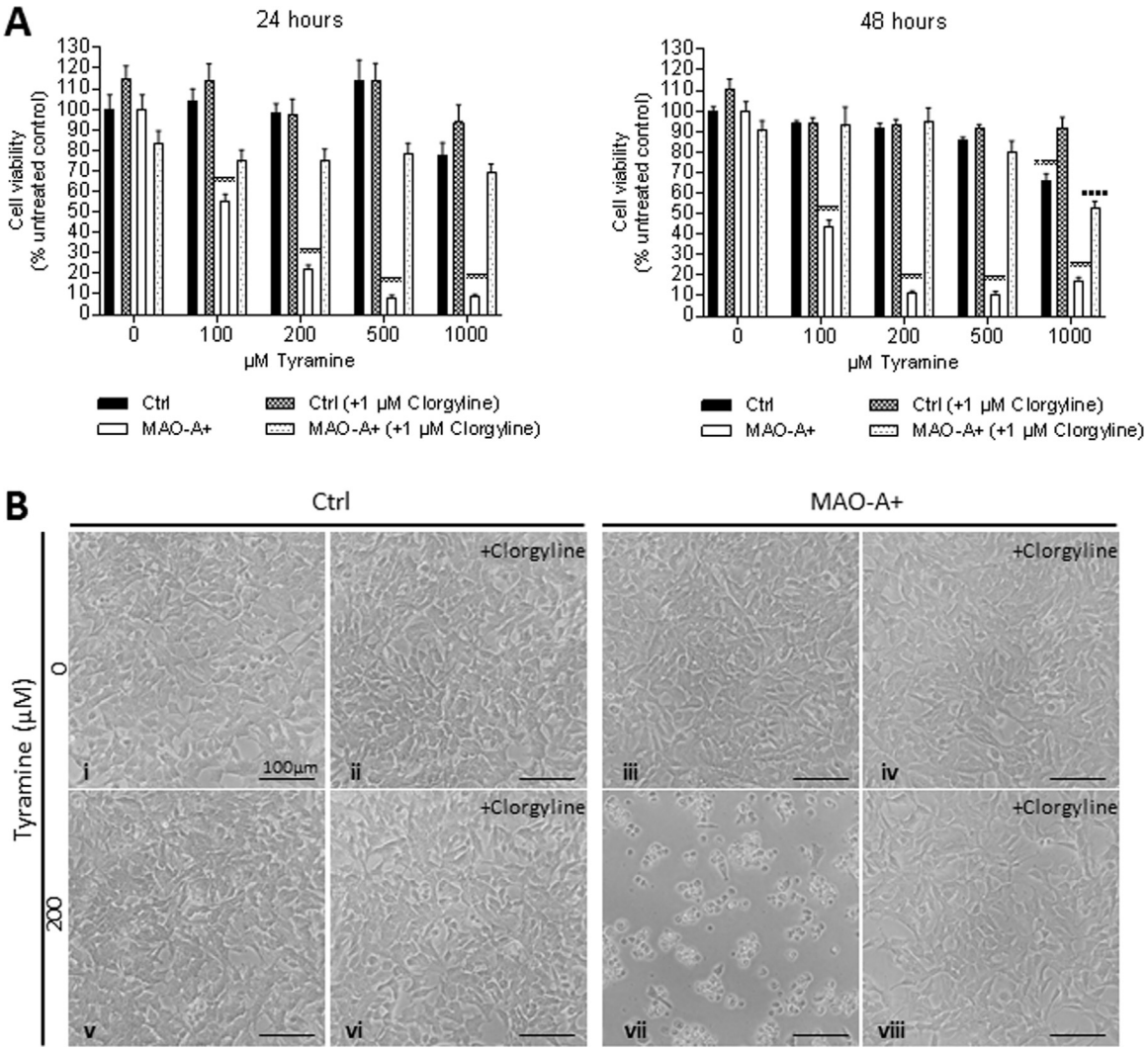

Fig. 8. Effects of excess MAO substrate availability on cell viability. (A) Cell viability quantified using the MTT reduction assays following 100 μM-1 mM tyramine exposure over a 48 h time course. Results were expressed as a percentage of untreated controls for both Ctrl and MAO-A+ cells, where n = 6–8. To inhibit MAO activity, cells were treated with clorgyline (1 μM), an irreversible MAO-A inhibitor for 30 min prior to addition of tyramine. Statistical significance for multiple comparisons was performed using a 2 way ANOVA followed by Bonferroni's multiple comparisons test. The effects of tyramine were assessed by comparing cell viability at each concentration to untreated controls (*$P < 0.05$, **$P < 0.01$, ****$p < 0.0001$). To assess the protective effect of MAO-A inhibition, clorgyline plus tyramine treated samples at each concentration were compared to clorgyline treatment only. Pre-treatment with clorgyline provided protection against the effects of tyramine at all concentration except the highest concentration (1 mM tyramine for 48 h, ****$p < 0.0001$). **(B)** Representative phase-contrast microscope images of Ctrl (panels i, ii, v and vi) and MAO-A+ (panels iii, iv, vii and viii) cells following 200 μM tyramine treatment for 48 h (panels v-viii). Addition of Clorgyline (+Clorgyline, panels ii, iv, vi and viii) reversed the detrimental effects of tyramine on MAO-A+ cells (note cell morphology shown in panel viii compared to panel vii).

investigated the levels of dynamin-1-like protein (drp1) and optic atrophy 1 (opa1), both known to regulate mitochondrial fission/fusion [36–38]. It is suggested that phosphorylation of drp1 on Ser 616 (p-drp1) promotes mitochondrial fission in neuronal cells under oxidative stress, whilst opa1, a mitochondrial inner membrane protein, is essential for mitochondrial fusion [39]. We found no significant changes in drp1 levels but increased levels of phosphorylated drp1 and reduced levels of opa1 in MAO-A+ cells (Fig. 6A), supporting mitochondrial fragmentation in MAO-A+ cells. Next, we tested whether MAO-A overexpression affected mitochondrial DNA (mtDNA) copy number. To do this we compared the levels of NADH-ubiquinone oxidoreductase chain 1 (ND1, mitochondrial) DNA relative to Beta-2-microglobulin (B2M, nuclear) DNA in control and MAO-A+ cells and found no significant differences in mtDNA copy number (Fig. 6B). We also investigated potential mtDNA deletions, but no deletions were detected (data not shown).

To investigate the effect of MAO-A overexpression on mitochondrial function, we initially measured mitochondrial membrane potential using the JC-1 fluorescent dye. JC-1 exhibits a mitochondrial potential dependent shift of fluorescence emission from green to red. Fluorescence spectrophotometric analysis showed that the ratio of red/green fluorescence intensity was not altered following sustained MAO-A over-expression (Fig. 6C). A protonophore carbonyl cyanide m-chlorophenylhydrazone (CCCP) was used as a positive control and, as expected, incubation with CCCP caused mitochondrial depolarisation in both control and MAO-A+ cells (Fig. 6C).

3.7. MAO-A overexpression results in increased complex IV activity

To further study the effect of MAO-A levels on mitochondrial function, we compared ETC activity in control and MAO-A+ cells. MAO-A overexpression resulted in significant elevation of basal complex IV activity with no significant effect on complex I, II, or III activities (Fig. 7A). We also found that citrate synthase activity (rate-limiting

enzyme in the tricarboxylic acid cycle) was similar in control and MAO-A+ cells, indicating that the change in complex IV activity was not due to a change in mitochondrial mass (Fig. 7A). To determine the nature of the mechanisms involved in the changes in mitochondrial metabolism in response to MAO-A expression, we focused on the abundance of mitochondrial protein components of distinct respiratory complexes. For this, we carried out a quantitative proteomics analysis, SWATH (Sequential window acquisition of all theoretical mass spectra) mass spectrometry (MS). SWATH is a recently developed technique, which performs label-free quantification by data-independent acquisition coupled with a peptide spectral library match. Using a minimum of 2 unique peptides we detected 7 complex IV subunits (of 19). Following stable MAO-A overexpression, there was a 1.43–2.58 fold increase in 6 complex IV subunits, with the lowest increase for COX4l1 and the largest for MT-CO2 (Fig. 7B).

Next, we investigated the ETC complex subunit levels using Western blotting. We found a small but significant increase in the levels of a nuclear encoded complex IV protein (COX4I1, 2 fold), and a much higher increase in mitochondrial encoded (MT-CO1 [4.4 fold] and MT-CO2 [8 fold]) complex IV subunits (Fig. 7C). In agreement with the ETC complex activity assays, MAO-A overexpression had no significant effect on the levels of complex II, III, V and citrate synthase protein levels. Mitochondrial encoded complex I subunit MT-ND1 levels were also investigated and found to be similar in control and MAO-A+ cells (Fig. 7C); suggesting increased mitochondrial encoded complex IV subunits were not due to a general up-regulation of mitochondrially encoded subunits. However, there was a small increase (1.6 fold) in a nuclear encoded complex I protein. Since there were no changes in citrate synthase activity levels, it also served as a loading control for the Western blot analysis.

Finally we investigated whether changes in the mitochondrial network and ETC activity affected cellular ATP levels and found total ATP levels to be similar in control and MAO-A+ cells (Fig. 7D). In order to investigate whether there was a change in the relative contributions of glycolysis and the ETC to ATP levels, we assessed ATP levels in the presence of glucose (total), or glucose and oligomycin (glycolysis), or 2-DG and pyruvate (ETC). There were no significant differences in glycolysis or ETC derived ATP in control and MAO-A+ cells (Fig. 7D). This finding suggests that increased complex IV activity contributes to the maintenance of energy supply.

3.8. Effects of MAO-A on cell viability depends on substrate availability

As MAO-A overexpression had no effect on ATP levels and caspase 3 activity, we finally checked the effect of providing excess MAO substrate on ability of cells to survive, knowing that levels of ROS produced by MAO will depend on substrate availability. We stimulated control and MAO-A+ cells with tyramine (100 μM to 1 mM) for 24 and 48 h. Tyramine had no effect on cell viability of control cells at 24 h (Fig. 8A). On the other hand, tyramine treatment caused significant cell death in MAO-A+ cells (Fig. 8A) starting at 100 μM. By 48 h, the highest concentration (1 mM) of tyramine also reduced viability of control cells. Clorgyline, an irreversible MAO-A inhibitor reversed the detrimental effects of tyramine on all cells (Figs. 8A and 8B) confirming downstream effects of MAO-A levels/activity depends on the substrate availability.

4. Discussion

Parkinson's disease is characterised by preferential degeneration of nigral dopaminergic neurons, resulting in dopamine deficiency. It is a complex disease and although its aetiology remains unclear, oxidative stress, mitochondrial dysfunction and altered proteolysis are considered important contributors to neurodegeneration in PD. Current symptomatic treatment of PD involves use of L-DOPA (dopamine precursor) alone or in combination with MAO-B inhibitors to maintain dopamine levels in the brain. In the human brain MAO-B is predominately located in glial cells and levels increase with age [40,41]. On the other hand, in neurons the metabolism of dopamine is undertaken largely by MAO-A, and nigral dopaminergic neurons solely express MAO-A [42]. Indeed studies carried out in animal models suggest both endogenously released and L-DOPA derived dopamine is mainly metabolised by MAO-A in the striatum [43,44].

Increased MAO-A expression/activities in dopaminergic neurons derived from induced pluripotent stem-cells from familial PD patients with mutations in parkin, glucocerebrosidase or α-synuclein have been reported [45–47]. Furthermore, a recent study by Tong et al., found increased levels of MAO-A protein fragments in the substantia nigra of Parkinson's disease post mortem brains, despite the loss of MAO-A containing neurons, supporting increased MAO-A expression (or turnover) in surviving dopaminergic neurons [48]. However, the downstream effects of increased MAO-A levels on neuronal cell death or survival have not been studied.

Our study involved SH-SY5Y neuroblastoma cells expressing higher levels of MAO-A protein (located on the mitochondrial outer membrane) and a relatively small increase in MAO-A activity. These cells produced a MAO-A mediated increase in ROS levels with associated increased cellular protein oxidation. Of interest MAO-A is highly resistant to short term exposure to H_2O_2 and this could be due to the fact that, out of 9 cysteine residues, only one (Cys - 406) is located in the active site and mutations in other residues do not alter catalytic activity [7,49,50]. The term 'mitochondrial ROS' is mainly used in reference to ROS produced by ETC but mitochondrial ROS can also be generated by enzymatic action of several other mitochondrial enzymes including MAOs. Indeed, studies carried out with intact mitochondria suggest H_2O_2 generated during deamination of tyramine by MAO is 48-fold higher than that generated during oxidation of succinate via complex II, again demonstrating the potential contribution of MAOs to cellular ROS levels and signalling [6].

It is now widely accepted that oxidative damage can result in increased demand for degradative turnover of damaged proteins (and organelles) and increasing evidence suggests ROS as an important signal involved in the activation of autophagy [17]. Recent research implicates a role for MAO-A in autophagy in prostate cancer cells and in cardiomyocytes but the results are conflicting [18,19]. MAO's potential role in a neuronal context has not been studied. Cellular quality control mechanisms are particularly important for neurons in order to maintain cellular homeostasis, and defects in autophagy are thought to be implicated in neurodegenerative disorders [49]. Of significance, we found that increased levels of MAO-A mediated cellular ROS promote autophagy to remove oxidatively damaged proteins/organelles and is likely to allow the MAO-A+ cells to survive and not to be apoptotic.

In addition to activation of autophagy our data demonstrate that increased MAO-A levels promote targeting of mitochondria for autophagic clearance. In MAO-A overexpressing cells the level of K63 ubiquitin chains was increased and K63 ubiquitination was associated with mitochondrial fractions, suggesting that mitochondria were specifically targeted for autophagic clearance. MAO-A overexpression resulted in an increased number of mitochondrial fragments whilst total mitochondrial network and volume per cell were maintained. Interestingly, there was no effect of MAO-A overexpression on overall mitochondrial membrane potential. This finding is in agreement with studies which reported that oxidative stress induced by H_2O_2 itself produces only a very slight reduction in mitochondrial membrane potential [50]. Although it is common practice to use mitochondrial uncouplers to trigger mitophagy (autophagy of mitochondria) in vitro, the physiological relevance of this approach in vivo has been questioned [51,52]. Here we show H_2O_2 generated locally on the mitochondrial outer membrane by MAO-A initiates mitochondrial fragmentation and clearance in the absence of mitochondrial uncouplers and mitochondrial depolarisation. In recent studies it has been demonstrated that mild oxidative stress and unfolded mitochondrial matrix proteins can

induce mitophagy in the absence of complete mitochondrial depolarisation [53,54]. Importantly, suppression of mitochondrial ROS signalling via high levels of catalase expression impairs activation of mitochondrial quality control mechanisms and compensatory autophagy [55]. Overall, our study adds to increasing evidence that mitophagy could be triggered without complete mitochondrial depolarisation and highlights MAO-A generated ROS as a potential mitochondrial quality control signal.

Whilst the ETC is regarded as one of the main sites that contributes to mitochondrial ROS generation, it has also been shown that ROS can damage and alter the activity of elements of the ETC [56]. In order to understand the effects of altered MAO-A levels on mitochondrial function, we investigated the activities and levels of ETC complexes. We found that MAO-A overexpression and associated increased ROS levels did not cause a reduction in activities of complexes I-IV. Significantly, for the first time we report that increased MAO-A levels result in increased complex IV activity/protein levels. It should be noted that the complex IV subunits MT-CO1 and MT-CO2, which are found to be highly upregulated in the MAO-A+ cells, are part of the catalytic core. MT-CO2 transfers the electrons from cytochrome c and is thought to be one of the major points of energy transduction and a key control point in the reaction. Since the overall cellular ATP levels were unchanged, the increase in complex IV activity could have a role in maintaining mitochondrial membrane potential and hence cellular energy needs.

We have previously demonstrated that inhibition of ETC complex I, III and IV, known to increase levels of mitochondrial ROS, leads to an increase in MAO-A protein [11]. Interestingly, a recent significant study by Stroud et al., reported increased MAO-A expression following knock down of accessory subunits of ETC complex I [57]. Importantly, the expression of only 20 mitochondrial proteins was altered, suggesting MAO-A is highly sensitive to changes in the ETC. Overall these observations suggest that there is a strong relationship between MAO-A levels and ETC activity, hence mitochondrial function.

Both autophagy and apoptosis can be induced by similar stimuli and there is a highly complex crosstalk between autophagy and apoptotic signal regulation [58]. Bcl-2 is suggested to be one of the key mediators of autophagy and apoptosis and its effect is dependent on its phosphorylation state [34,59]. Bcl-2 can sequester the autophagy activator Beclin 1, thus inhibiting autophagy but phosphorylation of Bcl-2 can disrupt this interaction. Stable overexpression of MAO-A led to no change in basal apoptosis, measured via caspase 3 activity, but stimulated autophagy concurrent with phosphorylation of Bcl-2 suggesting autophagy activation through disruption of Bcl-2/Beclin 1 interaction. However, other mechanisms, which was not investigated here, may also contribute to autophagy activation in MAO-A overexpressing cells. The aldehyde product of MAO deamination may lead to acidification of the cytosol and can contribute to induction of autophagy [60,61]. In addition, ROS produced by MAO activity can modify calcium signalling which in turn may also contribute to activation of autophagy [62,63]. It should be recognised that the effects of increased MAO-A levels will depend on availability of amine substrates and if the substrates are in excess, the cells may not be able to tolerate the increased ROS levels. Indeed exogenous addition of tyramine as substrate leads to a large reduction in viability of MAO-A overexpressing cells. This is particularly relevant to PD, where L-DOPA (dopamine precursor) is utilised to maintain dopamine levels in symptomatic treatment of PD [64].

This study is the first to show that an increase in MAO-A protein levels could lead to a protective cellular response in order to promote removal of damaged macromolecules/organelles via autophagy, but that amine substrate availability may ultimately determine cell fate. In addition, we provide further evidence that MAO-A plays a role in autophagy-apoptosis crosstalk and our findings support MAO-A as a key regulator of cell survival [11,19].

Acknowledgments

Authors thank Dr. Clare Coveney for her help with mass spectrometry analysis. This work was supported by Nottingham Trent University (UK). AUK is supported by Nottingham Trent University Independent Research Fellowship Scheme (UK). PYWM is supported by a Clinician Scientist Fellowship Award (G1002570) from the Medical Research Council (UK), and also receives funding from Fight for Sight (UK), the Isaac Newton Trust (UK), the UK National Institute of Health Research (NIHR) (UK) as part of the Rare Diseases Translational Research Collaboration, and the NIHR Biomedical Research Centre based at Moorfields Eye Hospital NHS Foundation Trust and UCL Institute of Ophthalmology.

Additional information

The authors declare that they have no conflicts of interest concerning this article.

References

[1] M.P. Murphy, How mitochondria produce reactive oxygen species, Biochem. J. (2009), https://doi.org/10.1042/BJ20081386.
[2] S.S. Sabharwal, P.T. Schumacker, Mitochondrial ROS in cancer: initiators, amplifiers or an achilles' heel? Nat. Rev. Cancer (2014), https://doi.org/10.1038/nrc3803.
[3] L.A. Sena, N.S. Chandel, Physiological roles of mitochondrial reactive oxygen species, Mol. Cell 48 (2012) 158–166, https://doi.org/10.1016/j.molcel.2012.09.025.
[4] P.R. Angelova, A.Y. Abramov, Functional role of mitochondrial reactive oxygen species in physiology, Free Radic. Biol. Med. (2016), https://doi.org/10.1016/j.freeradbiomed.2016.06.005.
[5] G. Paradies, G. Petrosillo, M. Pistolese, F.M. Ruggiero, Reactive oxygen species affect mitochondrial electron transport complex I activity through oxidative cardiolipin damage, Gene (2002) 135–141, https://doi.org/10.1016/S0378-1119(01)00814-9.
[6] N. Hauptmann, J. Grimsby, J.C. Shih, E. Cadenas, The metabolism of tyramine by monoamine oxidase A/B causes oxidative damage to mitochondrial DNA, Arch. Biochem. Biophys. 335 (1996) 295–304, https://doi.org/10.1006/abbi.1996.0510.
[7] A.W. Bach, N.C. Lan, D.L. Johnson, C.W. Abell, M.E. Bembenek, S.W. Kwan, P.H. Seeburg, J.C. Shih, cDNA cloning of human liver monoamine oxidase A and B: molecular basis of differences in enzymatic properties, Proc. Natl. Acad. Sci. USA 85 (1988) 4934–4938 〈http://www.pubmedcentral.nih.gov/articlerender.fcgi?artid=280552&tool=pmcentrez&rendertype=abstract〉.
[8] J.P. Johnson, Some observations upon a new inhibitor of monoamine oxidase in brain tissue, Biochem. Pharmacol. 17 (1968) 1285–1297, https://doi.org/10.1016/0006-2952(68)90066-X.
[9] M.L. christian Hare, Tyramine oxidase a new enzyme system in liver, Biochem J. 22 (1928) 968–979.
[10] J.P.M. Finberg, J.M. Rabey, Inhibitors of MAO-A and MAO-B in psychiatry and neurology, Front. Pharmacol. 7 (2016), https://doi.org/10.3389/fphar.2016.00340.
[11] J.C. Fitzgerald, A. Ugun-Klusek, G. Allen, L.A. De Girolamo, I. Hargreaves, C. Ufer, A.Y. Abramov, E.E. Billett, Monoamine oxidase-A knockdown in human neuroblastoma cells reveals protection against mitochondrial toxins, FASEB J. 28 (2014), https://doi.org/10.1096/fj.13-235481.
[12] G. Cohen, R. Farooqui, N. Kesler, Parkinson disease: a new link between monoamine oxidase and mitochondrial electron flow, Proc. Natl. Acad. Sci. USA 94 (1997) 4890–4894, https://doi.org/10.1073/pnas.94.10.4890.
[13] G.S. De Zutter, R.J. Davis, Pro-apoptotic gene expression mediated by the p38 mitogen-activated protein kinase signal transduction pathway, Proc. Natl. Acad. Sci. USA 98 (2001) 6168–6173, https://doi.org/10.1073/pnas.111027698.
[14] X.-M. Ou, K. Chen, J.C. Shih, Monoamine oxidase A and repressor R1 are involved in apoptotic signaling pathway, Proc. Natl. Acad. Sci. USA 103 (2006) 10923–10928, https://doi.org/10.1073/pnas.0601515103.
[15] J.C. Fitzgerald, C. Ufer, L.A. De Girolamo, H. Kuhn, E.E. Billett, Monoamine oxidase-A modulates apoptotic cell death induced by staurosporine in human neuroblastoma cells, J. Neurochem. 103 (2007) 2189–2199, https://doi.org/10.1111/j.1471-4159.2007.04921.x.
[16] X. Cao, L. Rui, P.R. Pennington, J. Chlan-Fourney, Z. Jiang, Z. Wei, X.M. Li, D.E. Edmondson, D.D. Mousseau, Serine 209 resides within a putativep38 (MAPK) consensus motif and regulates monoamine oxidase-A activity, J. Neurochem. 111 (2009) 101–110, https://doi.org/10.1111/j.1471-4159.2009.06300.x.
[17] J. Navarro-Yepes, M. Burns, A. Anandhan, O. Khalimonchuk, L.M. del Razo, B. Quintanilla-Vega, A. Pappa, M.I. Panayiotidis, R. Franco, Oxidative stress, redox signaling, and autophagy: cell death *versus* survival, Antioxid. Redox Signal. (2014), https://doi.org/10.1089/ars.2014.5837.
[18] Y. Santin, P. Sicard, F. Vigneron, C. Guilbeau-Frugier, M. Dutaur, O. Lairez, B. Couderc, D. Manni, V.I. Korolchuk, F. Lezoualc'h, A. Parini, J. Mialet-Perez, Oxidative stress by monoamine oxidase-A impairs transcription factor EB activation

and autophagosome clearance, leading to cardiomyocyte necrosis and heart failure, Antioxid. Redox Signal. 25 (2016) 10–27, https://doi.org/10.1089/ars.2015.6522.
[19] Y.-C. Lin, Y.-T. Chang, M. Campbell, T.-P. Lin, C.-C. Pan, H.-C. Lee, J.C. Shih, P.-C. Chang, MAOA-a novel decision maker of apoptosis and autophagy in hormone refractory neuroendocrine prostate cancer cells, Sci. Rep. 7 (2017) 46338, https://doi.org/10.1038/srep46338.
[20] D.B. Zorov, M. Juhaszova, S.J. Sollott, Mitochondrial reactive oxygen species (ROS) and ROS-induced ROS release, Physiol. Rev. (2014), https://doi.org/10.1152/physrev.00026.2013.
[21] L. He, P.F. Chinnery, S.E. Durham, E.L. Blakely, T.M. Wardell, G.M. Borthwick, R.W. Taylor, D.M. Turnbull, Detection and quantification of mitochondrial DNA deletions in individual cells by real-time PCR, Nucleic Acids Res. 30 (2002) e68, https://doi.org/10.1093/nar/gnf067.
[22] K.J. Krishnan, A. Bender, R.W. Taylor, D.M. Turnbull, A multiplex real-time PCR method to detect and quantify mitochondrial DNA deletions in individual cells, Anal. Biochem. 370 (2007) 127–129, https://doi.org/10.1016/j.ab.2007.06.024.
[23] F. Burte, L.A. De Girolamo, A.J. Hargreaves, E.E. Billett, Alterations in the mitochondrial proteome of neuroblastoma cells in response to complex 1 inhibition, J. Proteome Res. (2011), https://doi.org/10.1021/pr101211k.
[24] M. Spinazzi, A. Casarin, V. Pertegato, L. Salviati, C. Angelini, Assessment of mitochondrial respiratory chain enzymatic activities on tissues and cultured cells, Nat. Protoc. (2012) 1235–1246, https://doi.org/10.1038/nprot.2012.058 (TL-7, 7 VN-re).
[25] F.S. Vyas, A.J. Hargreaves, P.L.R. Bonner, D.J. Boocock, C. Coveney, J.M. Dickenson, A1 adenosine receptor-induced phosphorylation and modulation of transglutaminase 2 activity in H9c2 cells: a role in cell survival, Biochem. Pharmacol. (2016), https://doi.org/10.1016/j.bcp.2016.03.016.
[26] J.P. Lambert, G. Ivosev, A.L. Couzens, B. Larsen, M. Taipale, Z.Y. Lin, Q. Zhong, S. Lindquist, M. Vidal, R. Aebersold, T. Pawson, R. Bonner, S. Tate, A.C. Gingras, Mapping differential interactomes by affinity purification coupled with data-independent mass spectrometry acquisition, Nat. Methods 10 (2013) 1239–1245, https://doi.org/10.1038/nmeth.2702.
[27] E.E. Essick, F. Sam, Oxidative stress and autophagy in cardiac disease, neurological disorders, aging and cancer, Oxid. Med. Cell. Longev. 3 (2010) 168–177, https://doi.org/10.4161/oxim.3.3.2.
[28] R. Scherz-Shouval, E. Shvets, E. Fass, H. Shorer, L. Gil, Z. Elazar, Reactive oxygen species are essential for autophagy and specifically regulate the activity of Atg4, EMBO J. 26 (2007) 1749–1760, https://doi.org/10.1038/sj.emboj.7601623.
[29] D. Klionsky, L. Agholme, M. Agnello, P. Agostinis, J.A. Aguirre-ghiso, H.J. Ahn, O. Ait-mohamed, E.J. Brown, J.H. Brumell, N. Brunetti-pierri, U.T. Brunk, D.E. Bulman, S.J. Bultman, G. Bultynck, L.F. Burbulla, W. Bursch, J.P. Butchar, W. Buzgariu, S.P. Bydlowski, K. Cadwell, M. Cahová, D. Cai, J. Cai, Q. Cai, B. Calabretta, J. Calvo-garrido, N. Camougrand, M. Campanella, J. Campos-salinas, E. Candi, L. Cao, A.B. Caplan, S.R. Carding, S.M. Cardoso, J.S. Carew, C.R. Carlin, V. Carmignac, L.A.M. Carneiro, S. Carra, R.A. Caruso, G. Casari, C. Casas, R. Castino, E. Cebollero, F. Cecconi, J. Celli, H. Chaachouay, H. Chae, C. Chai, D.C. Chan, E.Y. Chan, R.C. Chang, C. Che, C. Chen, G. Chen, G. Chen, M. Chen, Q. Chen, S.S. Chen, W. Chen, X. Chen, X. Chen, X. Chen, Y. Chen, Y. Chen, Y. Chen, Y. Chen, Z. Chen, A. Cheng, C.H.K. Cheng, Y. Cheng, H. Cheong, J. Cheong, S. Cherry, R. Chess-williams, Z.H. Cheung, E. Chevet, H. Chiang, R. Chiarelli, T. Chiba, C.T. Chu, T. Chuang, S. Chueh, T. Chun, Y. Chwae, M. Chye, P. Codogno, H.A. Coller, M.I. Colombo, S. Comincini, M. Condello, F. Condorelli, S. Costes, A. Coto-montes, E. Couve, F.P. Coxon, J.M. Cregg, J.L. Crespo, L. Fésüs, R. Feuer, M.E. Figueiredo-pereira, G.M. Fimia, D.C. Fingar, S. Finkbeiner, Guidelines for the use and interpretation of assays for monitoring autophagy, Autophagy 8 (2016) 445–544, https://doi.org/10.4161/auto.19496.
[30] A. Yamamoto, Y. Tagawa, T. Yoshimori, Y. Moriyama, R. Masaki, Y. Tashiro, Bafilomycin A1 prevents maturation of autophagic vacuoles by inhibiting fusion between autophagosomes and lysosomes in rat hepatoma cell line, H-4-II-E cells, Cell Struct. Funct. 23 (1998) 33–42, https://doi.org/10.1247/csf.23.33.
[31] T. Yoshimori, a. Yamamoto, Y. Moriyama, M. Futai, Y. Tashiro, Bafilomycin-a1, a specific inhibitor of vacuolar-type H+-Atpase, inhibits acidification and protein-degradation in lysosomes of cultured-cells, J. Biol. Chem. 266 (1991) 17707–17712.
[32] S. Pankiv, T.H. Clausen, T. Lamark, A. Brech, J.A. Bruun, H. Outzen, A. Øvervatn, G. Bjørkøy, T. Johansen, p62/SQSTM1 binds directly to Atg8/LC3 to facilitate degradation of ubiquitinated protein aggregates by autophagy*[S], J. Biol. Chem. (2007), https://doi.org/10.1074/jbc.M702824200.
[33] S. Pattingre, A. Tassa, X. Qu, R. Garuti, H.L. Xiao, N. Mizushima, M. Packer, M.D. Schneider, B. Levine, Bcl-2 antiapoptotic proteins inhibit Beclin 1-dependent autophagy, Cell 122 (2005) 927–939, https://doi.org/10.1016/j.cell.2005.07.002.
[34] Y. Wei, S. Pattingre, S. Sinha, M. Bassik, B. Levine, JNK1-mediated phosphorylation of Bcl-2 regulates starvation-induced autophagy, Mol. Cell (2008), https://doi.org/10.1016/j.molcel.2008.06.001.
[35] J.M.M. Tan, E.S.P. Wong, D.S. Kirkpatrick, O. Pletnikova, H.S. Ko, S.P. Tay, M.W.L. Ho, J. Troncoso, S.P. Gygi, M.K. Lee, V.L. Dawson, T.M. Dawson, K.L. Lim, Lysine 63-linked ubiquitination promotes the formation and autophagic clearance of protein inclusions associated with neurodegenerative diseases, Hum. Mol. Genet. 17 (2008) 431–439, https://doi.org/10.1093/hmg/ddm320.
[36] E. Smirnova, L. Griparic, D.-L. Shurland, A.M. van der Bliek, Dynamin-related protein Drp1 is required for mitochondrial division in mammalian cells, Mol. Biol. Cell 12 (2001) 2245–2256, https://doi.org/10.1091/mbc.12.8.2245.
[37] A. Olichon, L.J. Emorine, E. Descoins, L. Pelloquin, L. Brichese, N. Gas, E. Guillou, C. Delettre, A. Valette, C.P. Hamel, B. Ducommun, G. Lenaers, P. Belenguer, The human dynamin-related protein OPA1 is anchored to the mitochondrial inner membrane facing the inter-membrane space, FEBS Lett. 523 (2002) 171–176, https://doi.org/10.1016/S0014-5793(02)02985-X.
[38] A.D. Mozdy, J.M. McCaffery, J.M. Shaw, Dnm1p GTPase-mediated mitochondrial fission is a multi-step process requiring the novel integral membrane component Fis1p, J. Cell Biol. 151 (2000) 367–379, https://doi.org/10.1083/jcb.151.2.367.
[39] X. Qi, M.-H. Disatnik, N. Shen, R.A. Sobel, D. Mochly-Rosen, Aberrant mitochondrial fission in neurons induced by protein kinase C{delta} under oxidative stress conditions in vivo, Mol. Biol. Cell 22 (2011) 256–265, https://doi.org/10.1091/mbc.E10-06-0551.
[40] C.J. Fowler, A. Wiberg, L. Oreland, J. Marcusson, B. Winblad, The effect of age on the activity and molecular properties of human brain monoamine oxidase, J. Neural Transm. 49 (1980) 1–20, https://doi.org/10.1007/BF01249185.
[41] J. Tong, J.H. Meyer, Y. Furukawa, I. Boileau, L.-J. Chang, A.A. Wilson, S. Houle, S.J. Kish, Distribution of monoamine oxidase proteins in human brain: implications for brain imaging studies, J. Cereb. Blood Flow Metab. 33 (2013) 863–871, https://doi.org/10.1038/jcbfm.2013.19.
[42] K.N. Westlund, R.M. Denney, R.M. Rose, C.W. Abell, Localization of distinct monoamine oxidase a and monoamine oxidase b cell populations in human brainstem, Neuroscience 25 (1988) 439–456, https://doi.org/10.1016/0306-4522(88)90250-3.
[43] J.P.M. Finberg, M.B.H. Youdim, Pharmacological properties of the anti-Parkinson drug rasagiline; modification of endogenous brain amines, reserpine reversal, serotonergic and dopaminergic behaviours, Neuropharmacology 43 (2002) 1110–1118, https://doi.org/10.1016/S0028-3908(02)00216-2.
[44] O. Sader-Mazbar, Y. Loboda, M.J. Rabey, J.P.M. Finberg, Increased L-DOPA-derived dopamine following selective MAO-A or -B inhibition in rat striatum depleted of dopaminergic and serotonergic innervation, Br. J. Pharmacol. 170 (2013) 999–1013, https://doi.org/10.1111/bph.12349.
[45] H. Jiang, Y. Ren, E.Y. Yuen, P. Zhong, M. Ghaedi, Z. Hu, G. Azabdaftari, K. Nakaso, Z. Yan, J. Feng, Parkin controls dopamine utilization in human midbrain dopaminergic neurons derived from induced pluripotent stem cells, Nat. Commun. 3 (2012), https://doi.org/10.1038/ncomms1669.
[46] B. Byers, B. Cord, H.N. Nguyen, B. Schüle, L. Fenno, P.C. Lee, K. Deisseroth, J.W. Langston, R.R. Pera, T.D. Palmer, SNCA triplication Parkinson's patient's iPSC-derived DA neurons accumulate α-synuclein and are susceptible to oxidative stress, PLoS One (2011), https://doi.org/10.1371/journal.pone.0026159.
[47] C.M. Woodard, B.A. Campos, S.H. Kuo, M.J. Nirenberg, M.W. Nestor, M. Zimmer, E.V. Mosharov, D. Sulzer, H. Zhou, D. Paull, L. Clark, E.E. Schadt, S.P. Sardi, L. Rubin, K. Eggan, M. Brock, S. Lipnick, M. Rao, S. Chang, A. Li, S.A. Noggle, IPSC-derived dopamine neurons reveal differences between monozygotic twins discordant for parkinson's disease, Cell Rep. 9 (2014) 1173–1182, https://doi.org/10.1016/j.celrep.2014.10.023.
[48] J. Tong, G. Rathitharan, J.H. Meyer, Y. Furukawa, L.C. Ang, I. Boileau, M. Guttman, O. Hornykiewicz, S.J. Kish, Brain monoamine oxidase B and A in human Parkinsonian dopamine deficiency disorders, Brain 140 (2017) 2460–2474, https://doi.org/10.1093/brain/awx172.
[49] R.A. Nixon, The role of autophagy in neurodegenerative disease, Nat. Med. (2013), https://doi.org/10.1038/nm.3232.
[50] C. Chinopoulos, L. Tretter, V. Adam-Vizi, Depolarization of in situ mitochondria due to hydrogen peroxide-induced oxidative stress in nerve terminals: inhibition of alpha-ketoglutarate dehydrogenase, J. Neurochem. (1999), https://doi.org/10.1046/j.1471-4159.1999.0730220.x.
[51] A.J. Whitworth, L.J. Pallanck, PINK1/Parkin mitophagy and neurodegeneration—what do we really know in vivo? Curr. Opin. Genet. Dev. (2017), https://doi.org/10.1016/j.gde.2017.01.016.
[52] T.G. McWilliams, A.R. Prescott, G.F.G. Allen, J. Tamjar, M.J. Munson, C. Thomson, M.M.K. Muqit, I.G. Ganley, Mito-QC illuminates mitophagy and mitochondrial architecture in vivo, J. Cell Biol. (2016), https://doi.org/10.1083/jcb.201603039.
[53] S.M. Jin, R.J. Youle, The accumulation of misfolded proteins in the mitochondrial matrix is sensed by PINK1 to induce PARK2/Parkin-mediated mitophagy of polarized mitochondria, Autophagy 9 (2013) 1750–1757, https://doi.org/10.4161/auto.26122.
[54] M. Frank, S. Duvezin-Caubet, S. Koob, A. Occhipinti, R. Jagasia, A. Petcherski, M.O. Ruonala, M. Priault, B. Salin, A.S. Reichert, Mitophagy is triggered by mild oxidative stress in a mitochondrial fission dependent manner, Biochim. Biophys. Acta – Mol. Cell Res. (2012), https://doi.org/10.1016/j.bbamcr.2012.08.007.
[55] M. Song, Y. Chen, G. Gong, E. Murphy, P.S. Rabinovitch, G.W. Dorn, Super-suppression of mitochondrial reactive oxygen species signaling impairs compensatory autophagy in primary mitophagic cardiomyopathy, Circ. Res. (2014), https://doi.org/10.1161/CIRCRESAHA.115.304384.
[56] A. Musatov, N.C. Robinson, Susceptibility of mitochondrial electron-transport complexes to oxidative damage. Focus on cytochrome c oxidase, Free Radic. Res. (2012), https://doi.org/10.3109/10715762.2012.717273.
[57] D.A. Stroud, E.E. Surgenor, L.E. Formosa, B. Reljic, A.E. Frazier, M.G. Dibley, L.D. Osellame, T. Stait, T.H. Beilharz, D.R. Thorburn, A. Salim, M.T. Ryan, Accessory subunits are integral for assembly and function of human mitochondrial complex I, Nature (2016), https://doi.org/10.1038/nature19754.
[58] G. Mariño, M. Niso-Santano, E.H. Baehrecke, G. Kroemer, Self-consumption: the interplay of autophagy and apoptosis, Nat. Rev. Mol. Cell Biol. (2014), https://doi.org/10.1038/nrm3735.
[59] T. Ito, X. Deng, B. Carr, W.S. May, Bcl-2 phosphorylation required for anti-apoptosis function, J. Biol. Chem. (1997), https://doi.org/10.1074/jbc.272.18.11671.
[60] H. Legros, M.G. Dingeval, F. Janin, J. Costentin, J.J. Bonnet, Toxicity of a treatment associating dopamine and disulfiram for catecholaminergic neuroblastoma SH-SY5Y cells: relationships with 3,4-dihydroxyphenylacetaldehyde formation, Neurotoxicology (2004), https://doi.org/10.1016/S0161-813X(03)00148-7.
[61] A.V. Berezhnov, M.P.M. Soutar, E.I. Fedotova, M.S. Frolova, H. Plun-Favreau, V.P. Zinchenko, A.Y. Abramov, Intracellular pH modulates autophagy and

mitophagy, J. Biol. Chem. (2016), https://doi.org/10.1074/jbc.M115.691774.
[62] A. Vaarmann, S. Gandhi, A.Y. Abramov, Dopamine induces Ca^{2+} signaling in astrocytes through reactive oxygen species generated by monoamine oxidase, J. Biol. Chem. (2010), https://doi.org/10.1074/jbc.M110.111450.
[63] M.D. Bootman, T. Chehab, G. Bultynck, J.B. Parys, K. Rietdorf, The regulation of autophagy by calcium signals: do we have a consensus? Cell Calcium (2017), https://doi.org/10.1016/j.ceca.2017.08.005.
[64] P. Riederer, G. Laux, MAO-inhibitors in Parkinson's disease, Exp. Neurobiol. 20 (2011) 1, https://doi.org/10.5607/en.2011.20.1.1.